



pyisotopomer: A Python package for obtaining intramolecular isotope ratio differences from mass spectrometric analysis of nitrous oxide isotopocules

Journal:	<i>Rapid Communications in Mass Spectrometry</i>
Manuscript ID	RCM-23-0010.R1
Wiley - Manuscript type:	Protocol
Date Submitted by the Author:	21-Mar-2023
Complete List of Authors:	Kelly, Colette; Stanford University, Earth System Science Manning, Cara; University of Connecticut, Department of Marine Sciences; University of Connecticut, Department of Marine Sciences Frey, Claudia; University of Basel Kaiser, Jan; University of East Anglia, School of Environmental Sciences Gluschankoff, Noah; Stanford University, Earth System Science Casciotti, Karen; Stanford University, Department of Earth System Science
Keywords:	Nitrous oxide, isotopomers, isotopocules, scrambling, Python
Abstract:	<p>RATIONALE Obtaining nitrous oxide isotopocule measurements with isotope ratio mass spectrometry (IRMS) involves analyzing the ion current ratios of the nitrous oxide parent ion (N_2O^+) as well as those of the NO^+ fragment ion. The data analysis requires correcting for "scrambling" in the ion source, whereby the NO^+ fragment ion obtains the outer N atom from the N_2O^+ molecule. While descriptions exist for this correction, and interlaboratory intercalibration efforts have been made, there has yet to be published a package of code for implementing isotopomer calibrations.</p> <p>METHODS We developed a user-friendly Python package (pyisotopomer) to determine two coefficients (γ and κ) that describe scrambling in the IRMS ion source, and then to use this calibration to obtain intramolecular isotope deltas in N_2O samples.</p> <p>RESULTS With two appropriate reference materials, γ and κ can be determined robustly and accurately for a given IRMS. An additional third reference material is needed to define the zero-point of the delta scale. We show that IRMS scrambling behavior can vary with time, necessitating regular calibrations. Finally, we present an intercalibration between two IRMS laboratories, using pyisotopomer to calculate γ and κ and to obtain intramolecular N_2O isotope deltas in lake water unknowns.</p> <p>CONCLUSIONS Given these considerations, we discuss how to use pyisotopomer to obtain high-quality N_2O isotopocule data from IRMS</p>

1
2
3
4
5
6
7
8
9
10
11
12
13
14
15
16
17
18
19
20
21
22
23
24
25
26
27
28
29
30
31
32
33
34
35
36
37
38
39
40
41
42
43
44
45
46
47
48
49
50
51
52
53
54
55
56
57
58
59
60

	systems, including the use of appropriate reference materials and frequency of calibration.

SCHOLARONE™
Manuscripts

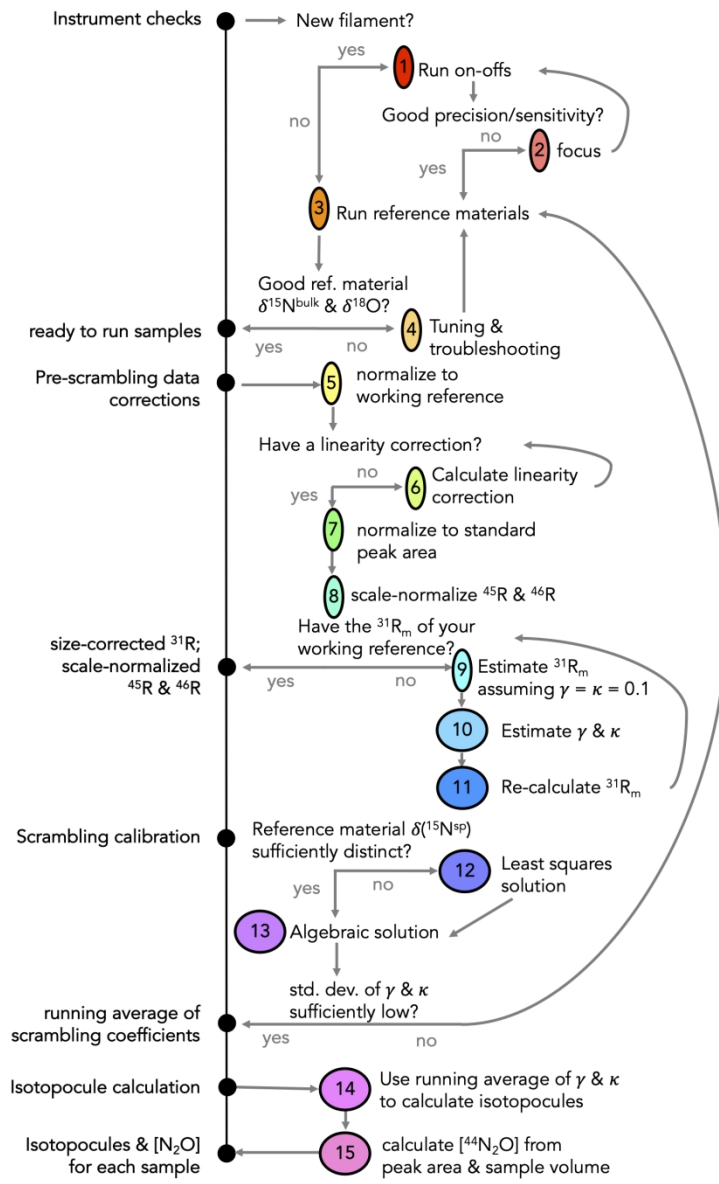


Figure 1. N₂O data corrections flowchart. Instrument checks, pre-scrambling data corrections, the scrambling calibration, and isotopomer calculations are laid out; numbers in yellow circles correspond to step numbers referred to in the text. Steps 1-4 are performed with raw Isodat output, steps 5-8 are accomplished in the data corrections spreadsheet template, step 9 is a simple calculation, and steps 10-14 are accomplished with the pisisotopomer code.

558x914mm (72 x 72 DPI)

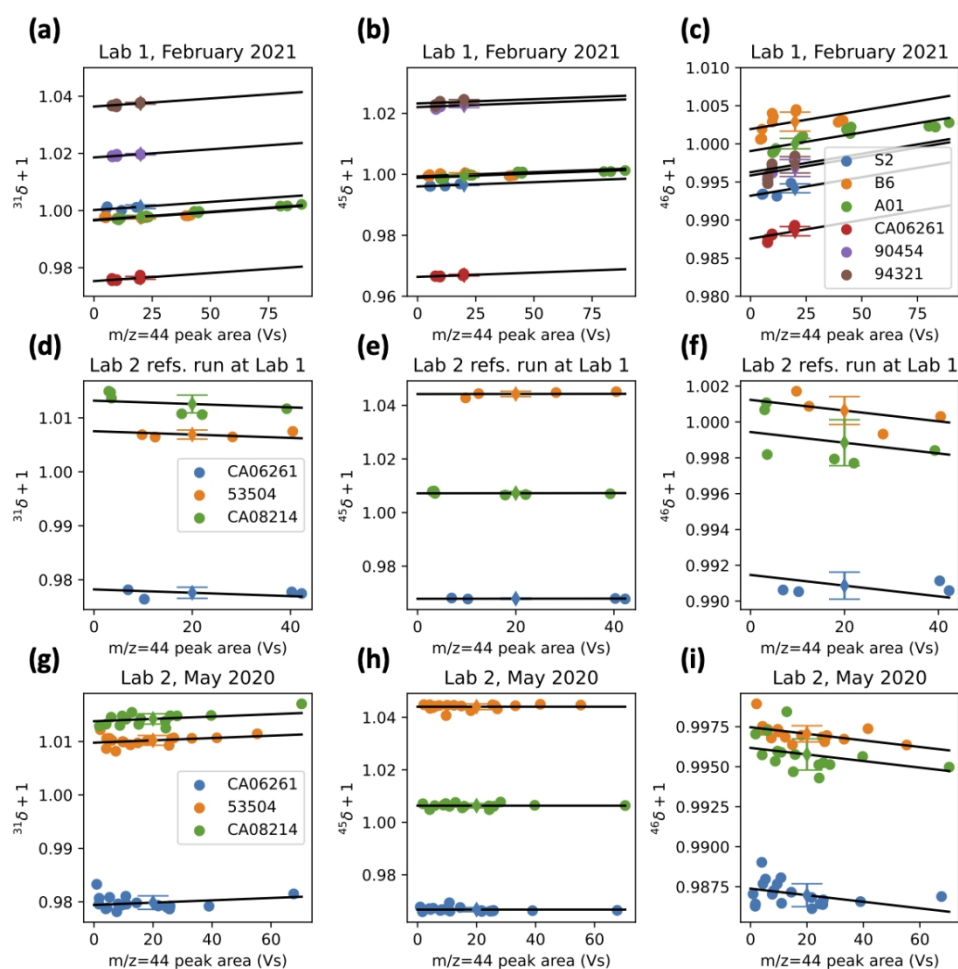


Figure 2. Linearity relations for reference materials used to normalize measured isotope ratios to a peak area of 20 Vs (10 nmol N₂O), using the dummy variable method. $^{31}\delta+1$ (a,d,g), $^{45}\delta+1$ (b,e,h), and $^{46}\delta+1$ (c, f, i) are plotted against m/z 44 peak area. Linearity relations are shown for reference materials prepared and run in Lab 1 (a-c), reference materials prepared in Lab 2 but run in Lab 1 (d-f), and reference materials run in Lab 2 (g-i). A common slope (black line) calculated from the dummy variable method for each molecular ion ratio is overlain on each data series (colored circles). The estimated isotope ratio corresponding to a peak area of 20 Vs is also shown for each series (colored diamonds, error bars correspond to the standard error of the predicted y-value).

431x431mm (72 x 72 DPI)

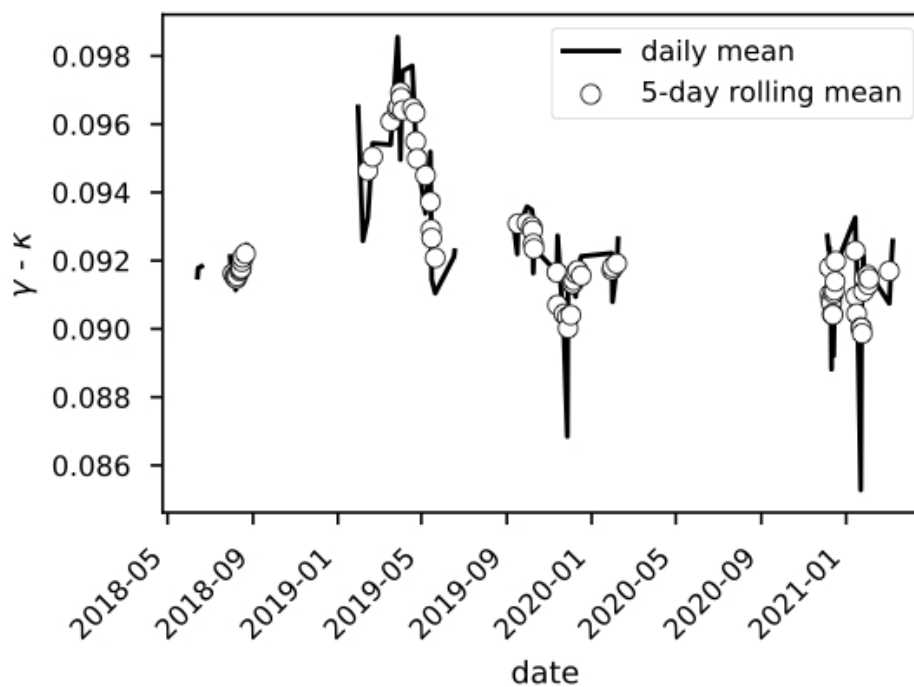


Figure 3. $\gamma - \kappa$ for the Lab 1 IRMS from June 2018 to March 2021. Daily mean $\gamma - \kappa$ (black line) values are plotted with a 5-day rolling average (dots).

203x152mm (72 x 72 DPI)

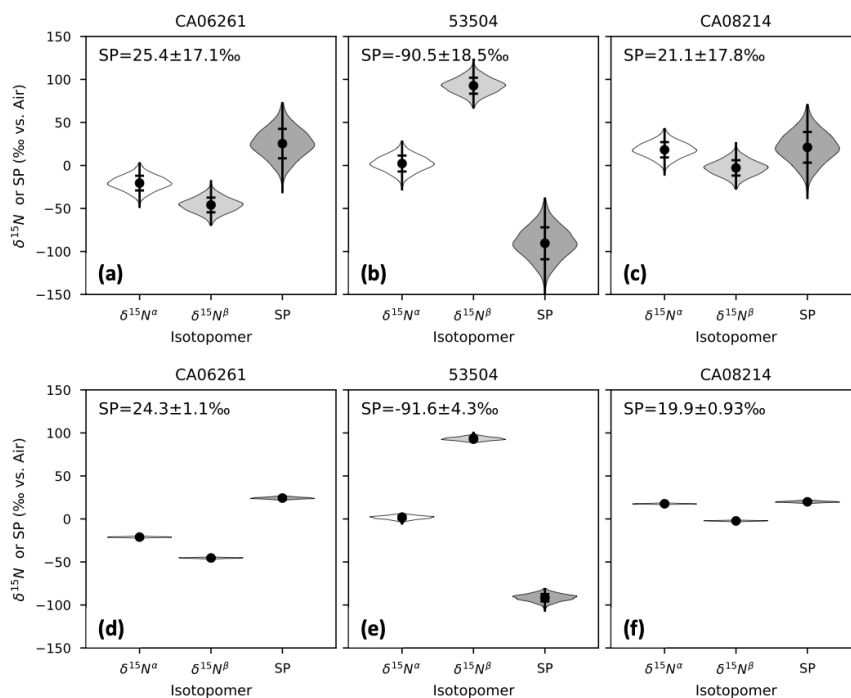


Figure 4. a-c) Isotopocule values and error associated with a 10 % relative uncertainty in $\gamma - \kappa$, based on Monte Carlo simulation results, for reference materials CA062621 (a), 53504 (b), and CA08214 (c). γ and κ were modeled as random numbers centered around $\gamma = 0.174$ and $\kappa = 0.083$, with the uncertainty in $\gamma - \kappa$ equal to 10 % of the mean (0.091). d-f) Isotopocule values and error associated with a 10% relative uncertainty in the absolute values of $\gamma - \kappa$, holding $\gamma - \kappa$ constant, for reference materials CA062621 (d), 53504 (e), and CA08214 (f). γ and κ were modeled in tandem as random numbers centered around $\gamma = 0.174$ and $\kappa = 0.083$, with uncertainties equal to 10% of the mean γ , and $\gamma - \kappa$ was held constant at 0.091. Violin plots are based on a kernel density estimate of the distribution and the values plotted and reported on each figure show the mean value $\pm 1\sigma$.

431x304mm (72 x 72 DPI)

1
2
3
4
5
6
7
8
9
10
11
12
13
14
15
16
17
18
19
20
21
22
23
24
25
26
27
28
29
30
31
32
33
34
35
36
37
38
39
40
41
42
43
44
45
46
47
48
49
50
51
52
53
54
55
56
57
58
59
60

In preparation for Rapid Communications in Mass Spectrometry
pyisotopomer: A Python package for obtaining intramolecular isotope ratio differences from mass spectrometric analysis of nitrous oxide isotopocules
Colette L. Kelly,^{1*} Cara Manning,² Claudia Frey,³ Jan Kaiser,⁴ Noah Gluschankoff,¹ and Karen L. Casciotti

6 1. Stanford University, Department of Earth System Science, Stanford, CA 94305, USA
7 2. University of Connecticut, Department of Marine Sciences, Groton, CT, 06340, USA
8 3. Department of Environmental Science, University of Basel, Basel, Switzerland.
9 4. University of East Anglia, Centre for Ocean and Atmospheric Sciences, School of
10 Environmental Sciences, Norwich, NR4 7TJ, UK

11
12 * **Correspondence to:** Colette L. Kelly (email: clkelly@stanford.edu; phone: 802-595-3647;
13 address: 473 Via Ortega Room 140, Stanford, CA 94305).

14
15 **Keywords:** Nitrous oxide, isotopomers, isotopocules, scrambling, Python

16 17 **Abstract**

18
19 **RATIONALE** Obtaining nitrous oxide isotopocule measurements with isotope ratio mass
20 spectrometry (IRMS) involves analyzing the ion current ratios of the nitrous oxide parent ion
21 (N_2O^+) as well as those of the NO^+ fragment ion. The data analysis requires correcting for
22 “scrambling” in the ion source, whereby the NO^+ fragment ion obtains the outer N atom from the
23 N_2O molecule. While descriptions exist for this correction, and interlaboratory intercalibration
24 efforts have been made, there has yet to be published a package of code for implementing
25 isotopomer calibrations.

26
27 **METHODS** We developed a user-friendly Python package (pyisotopomer) to determine two
28 coefficients (γ and κ) that describe scrambling in the IRMS ion source, and then to use this
29 calibration to obtain intramolecular isotope deltas in N_2O samples.
30

31 **RESULTS** With two appropriate reference materials, γ and κ can be determined robustly and
32 accurately for a given IRMS. An additional third reference material is needed to define the zero-
33 point of the delta scale. We show that IRMS scrambling behavior can vary with time,
34 necessitating regular calibrations. Finally, we present an intercalibration between two IRMS
35 laboratories, using pyisotopomer to calculate γ and κ , and to obtain intramolecular N_2O isotope
36 deltas in lake water unknowns.
37

38 **CONCLUSIONS** Given these considerations, we discuss how to use pyisotopomer to obtain
39 high-quality N_2O isotopocule data from IRMS systems, including the use of appropriate
40 reference materials and frequency of calibration.

1. Introduction

Nitrous oxide (N₂O) is a potent greenhouse gas, with a global warming potential 265 times that of carbon dioxide over a 100 year time horizon^{1,2}. N₂O is also likely to be the most emitted ozone depletion agent in the 21st century, due to production of NO radicals in the stratosphere that interact destructively with ozone³⁻⁶. Historically, the bulk stable isotopes of nitrogen and oxygen in N₂O have been used to quantify its microbial cycling in soils^{7,8} and in the ocean⁹⁻¹², its destruction by photolysis and O(¹D), and its cycling in the atmosphere^{13,14}. This approach often fails at disentangling different N₂O production and consumption mechanisms, because the bulk nitrogen and oxygen isotope ratios of N₂O depend on the isotopic composition of the substrate, as well as the isotope effects of production and consumption processes¹². Furthermore, in the context of microbial N₂O cycling in soils and the ocean, bacterial nitrification and denitrification produce N₂O with similar bulk $\delta(^{15}\text{N})$ ¹ values, preventing partitioning between these processes on the basis of bulk $\delta(^{15}\text{N})$ alone^{15,16}.

The site-specific nitrogen isotope ratios of N₂O provide a more nuanced constraint on the biogeochemical cycling of N₂O than its bulk composition alone. N₂O isotopomers have been used extensively to quantify its biogeochemical cycling in soils¹⁷⁻²⁰, the atmosphere^{14,21-23}, and the ocean²⁴⁻³⁴. The individual isotopic compositions of each nitrogen atom were first measured by Friedman and Bigeleisen, who quantified the yields of isotopomers ¹⁴N¹⁵N¹⁶O and ¹⁵N¹⁴N¹⁶O from enriched ammonium nitrate by measuring the NO⁺ fragment ion signal in an isotope ratio mass spectrometer (IRMS)³⁵. 50 years later, these N₂O isotopomers were quantified at natural abundance from the N₂O⁺ species with mass numbers 44, 45, and 46 and the mass 30 and 31 NO⁺ fragment ion^{36,37}. The central nitrogen atom in the N₂O molecule has been designated with locants α , μ , or 2; the terminal atom, with locants β , τ , or 1^{38,39}. Here, we use the definitions from Toyoda and Yoshida (1999) for the site-specific isotope number (N) ratios of the central (α) nitrogen atom and terminal (β) nitrogen atom³⁶:

$${}^{15}R^{\alpha} = \frac{N(^{14}\text{N}^{15}\text{NO})}{N(^{14}\text{N}^{14}\text{NO})} \quad (1)$$

$${}^{15}R^{\beta} = \frac{N(^{15}\text{N}^{14}\text{NO})}{N(^{14}\text{N}^{14}\text{NO})} \quad (2)$$

The N₂O isotopomer measurement was initially performed with two sequential measurements of the same sample on an isotope ratio mass spectrometer, one at m/z 44, 45, and 46, and the other at m/z 30 and 31³⁶. Use of dedicated cup-configurations on lower-dispersion IRMS instruments allowed simultaneous analysis of all five masses together⁴⁰.

The slight difference in absorption cross sections between the isotopocules of N₂O result in different isotopic fractionations during photolysis and photo-oxidation in the stratosphere⁴¹, making the isotopomers of N₂O a powerful tool for understanding its atmospheric cycling^{21,42-45}. Likewise, N₂O site preference, defined as $\delta(^{15}\text{N}^{\text{sp}}) = \delta(^{15}\text{N}^{\alpha}) - \delta(^{15}\text{N}^{\beta})$, was shown in microbial culture experiments to be largely a function of reaction mechanism, independent of source composition^{24,46-50}. This allowed for the differentiation between N₂O from bacterial nitrification ($\delta(^{15}\text{N}^{\text{sp}}) \approx 28\text{-}38\text{‰}$) and denitrification ($\delta(^{15}\text{N}^{\text{sp}}) \approx 0$)^{24,46-50}, although more studies are needed

¹ We write δ values with parentheses, e.g., $\delta(^{15}\text{N})$, because δ is the quantity symbol and “¹⁵N” is the label. See SI Brochure: <https://www.bipm.org/en/publications/si-brochure/>

to better constrain the SPs for diverse fungal, bacterial, and archaeal strains in both terrestrial and marine environments^{49,51}. During N₂O consumption, $\delta(^{15}\text{N}^\alpha)$ and $\delta(^{18}\text{O})$ were shown in microbial culture⁵² and soil mesocosm¹⁹ experiments to exhibit a characteristic relationship, allowing subsequent studies to use this relationship to distinguish between oxidative and reductive regimes of N₂O cycling^{30,33}.

Site-specific nitrogen isotope ratio measurements based on mass spectrometry need to be corrected for a phenomenon called “scrambling,” whereby the NO⁺ fragment ion contains the terminal N atom, rather than the central N attached to the O atom (as in the original molecule). A number of approaches have been taken to calibrate an IRMS system for this effect: 1) the use of a single “rearrangement factor” to describe scrambling^{36,53}, 2) the use of nine coefficients to describe the different fragmentation behaviors of the different isotopocules of N₂O⁵⁴, and finally 3) the use of two coefficients to describe scrambling in the ion source⁵⁰. While descriptions exist for each of these approaches, and interlaboratory intercalibration efforts have been made^{55,56}, there has yet to be published a package of code for implementing any of the above isotopomer calibrations.

We developed a Python software package (“pyisotopomer”) that implements the two-coefficient approach described by Frame and Casciotti³² to calibrate an IRMS for scrambling and use that calibration to obtain high-quality N₂O isotopocule data. This software solves a set of equations, either analytically or with an optimization routine, to quantify the scrambling behavior of an IRMS. To quantify the performance of the software, we tested the sensitivity of the analytical and optimization-based solutions to their input conditions and assessed when each method is most appropriate. To quantify the variability of the fragmentation behavior of an instrument over time, we examined the scrambling behavior of one IRMS over the course of four years of measurements. We derived a simplified equation and used a Monte Carlo simulation approach to quantify the effect of uncertainty in the scrambling coefficients on the final isotope deltas. Finally, we performed an intercalibration using this software across two labs, at Stanford University (‘Lab 1’) and the University of Basel (‘Lab 2’). This paper introduces the theory, practical applications, and testing of pyisotopomer; instructions on how to use pyisotopomer are available in the documentation on the Python Package Index⁵⁷.

2. Mathematical framework

The molecular ion number ratios 45/44 (⁴⁵R) and 46/44 (⁴⁶R) can be written in terms of atomic isotope ratios as^{36,53}:

$$^{45}R = ^{15}R^\alpha + ^{15}R^\beta + ^{17}R \quad (3)$$

$$^{46}R = (^{15}R^\alpha + ^{15}R^\beta)^{17}R + ^{18}R + ^{15}R^\alpha ^{15}R^\beta \quad (4)$$

where ¹⁵R^α, ¹⁵R^β, ¹⁷R and ¹⁸R denote the number ratios of ¹⁴N¹⁵N¹⁶O, ¹⁵N¹⁴N¹⁶O, ¹⁴N₂¹⁷O, and ¹⁴N₂¹⁸O, respectively, to ¹⁴N₂¹⁶O, assuming a stochastic isotope distribution between mono- and poly-substituted isotopocules.

For many N₂O samples, ¹⁷R covaries with ¹⁸R according to the oxygen isotope ratios of Vienna Standard Mean Ocean Water (VSMOW)^{58,59} and a mass-dependent relationship between ¹⁷R and ¹⁸R with coefficient $\beta = 0.516$ ⁶⁰. Deviations from this relationship are expressed by the oxygen triple isotope excess $\Delta(^{17}\text{O})$ ^{60–62}, which provides additional information about the sources and sinks of N₂O^{60,63}:

$$^{17}R/^{17}R_{\text{VSMOW}} = (^{18}R/0.0020052)^{\beta}[\Delta(^{17}\text{O}) + 1] \quad (5)$$

$\Delta(^{17}\text{O})$ is sometimes assumed to be equal to zero but should be measured separately for samples with a significant $\Delta(^{17}\text{O})$ anomaly, such as atmospheric nitrate^{60,62,63}.

The simplest formulation for the NO^+ fragment ion number ratio 31/30 (^{31}R) is given as³⁶:

$$^{31}R = ^{15}R^{\alpha} + ^{17}R \quad (6)$$

This equation would represent the ^{31}R measured by IRMS if no scrambling occurred.

To describe instead the scrambled ^{31}R , Toyoda and Yoshida³⁶ define the rearrangement factor γ (which was later given the symbol γ) as “the fraction of NO^+ bearing the β nitrogen of the initial N_2O to the total NO^+ formed,” to yield:

$$^{31}R = (1 - \gamma)^{15}R^{\alpha} + \gamma^{15}R^{\beta} + ^{17}R \quad (7)$$

where $^{15}R^{\alpha}$ and $^{15}R^{\beta}$ represent atomic isotope ratios of the sample. In other words, γ relates the scrambled NO^+ fragment ratio to the unscrambled $^{15}R^{\alpha}$ and $^{15}R^{\beta}$ of the sample.

Kaiser et al.⁵³ introduced a more complete representation of ^{31}R , adding terms for $^{15}\text{N}^{15}\text{N}^{16}\text{O}$, $^{14}\text{N}^{15}\text{N}^{17}\text{O}$, and $^{15}\text{N}^{14}\text{N}^{17}\text{O}$ to m/z 31, and terms for $^{15}\text{N}^{14}\text{N}^{16}\text{O}$ and $^{14}\text{N}^{15}\text{N}^{16}\text{O}$ to m/z 30:

$$\begin{aligned} ^{31}R &= (1 - \gamma)^{15}R^{\alpha} + \gamma^{15}R^{\beta} + ^{17}R - \frac{\gamma(1 - \gamma)(^{15}R^{\alpha} - ^{15}R^{\beta})^2}{1 + \gamma^{15}R^{\alpha} + (1 - \gamma)^{15}R^{\beta}} \quad (8) \\ &= \frac{(1 - \gamma)^{15}R^{\alpha} + \gamma^{15}R^{\beta} + ^{15}R^{\alpha}{}^{15}R^{\beta} + ^{17}R[1 + \gamma^{15}R^{\alpha} + (1 - \gamma)^{15}R^{\beta}]}{1 + \gamma^{15}R^{\alpha} + (1 - \gamma)^{15}R^{\beta}} \end{aligned}$$

Note that Kaiser et al.⁵³ use the symbol “ s ” for γ , $^{15}R_1$ for $^{15}R^{\beta}$, and $^{15}R_2$ for $^{15}R^{\alpha}$.

To account for different fragmentation rates of different N_2O isotopocules, Westley et al.⁵⁴ replaced the rearrangement factor γ with nine separate coefficients:

$$^{31}R = \frac{a_{31}^{15}R^{\alpha} + b_{31}^{15}R^{\beta} + c_{31}^{15}R^{\alpha}{}^{15}R^{\beta} + ^{17}R[d_{31} + e_{31}^{15}R^{\alpha} + f_{31}^{15}R^{\beta}]}{1 + a_{30}^{15}R^{\alpha} + b_{30}^{15}R^{\beta} + c_{30}^{15}R^{\alpha}{}^{15}R^{\beta}} \quad (9)$$

While this approach considers the possibility of different rearrangement factors for every N_2O isotopocule as well as $^{15}\text{N}_2^+$ formation, it also requires solving for three to nine coefficients, depending on whether a_{30} , b_{30} and c_{30} , as well as d_{31} , e_{31} and f_{31} , are considered separately from coefficients a_{31} , b_{31} and c_{31} .

Frame and Casciotti⁵⁰ simplify this equation by reducing the number of rearrangement factors to two coefficients, γ and κ , which represent the yield of $^{14}\text{NO}^+$ from $^{14}\text{N}^{15}\text{N}^{16}\text{O}$ and $^{14}\text{N}^{15}\text{N}^{17}\text{O}$, and the yield of $^{15}\text{NO}^+$ from $^{15}\text{N}^{14}\text{N}^{16}\text{O}$, respectively. This produces the equation:

$$^{31}R = \frac{(1 - \gamma)^{15}R^{\alpha} + \kappa^{15}R^{\beta} + ^{15}R^{\alpha}{}^{15}R^{\beta} + ^{17}R[1 + \gamma^{15}R^{\alpha} + (1 - \kappa)^{15}R^{\beta}]}{1 + \gamma^{15}R^{\alpha} + (1 - \kappa)^{15}R^{\beta}} \quad (10)$$

The important pieces of information contained within the two scrambling factors are the unequal rates of fragmentation for the isotopomers $^{14}\text{N}^{15}\text{NO}$ and $^{15}\text{N}^{14}\text{NO}$, which eqns. (7) and (8) assume are equal. Eqn. (10) is formulated by assuming that the ^{17}O -isotopocules have the same scrambling behavior as the ^{16}O -isotopocules, i.e., $e_{31} = 1 - a_{31}$ and $f_{31} = 1 - b_{31}$, in terms of the coefficients in eqn. (9). It is also assumed that $c_{31} = 1$, i.e., the yield of $^{15}\text{N}^{16}\text{O}^+$ from $^{15}\text{N}_2^{16}\text{O}$ is equal to the yield of $^{14}\text{N}^{16}\text{O}^+$ from $^{14}\text{N}_2^{16}\text{O}$. Given that naturally occurring N_2O contains very

149 little $^{15}\text{N}_2^{16}\text{O}$, a small difference in this yield would not significantly alter $^{31}\text{R}^{64}$. Finally, it is
 150 assumed that $d_{31} = 1$, or that the yield of $^{14}\text{N}^{17}\text{O}^+$ from $^{14}\text{N}_2^{17}\text{O}$ is equal to the yield of $^{14}\text{N}^{16}\text{O}^+$
 151 from $^{14}\text{N}_2^{16}\text{O}$; again, an assumption yielding little error in ^{31}R , given the low natural abundance
 152 of ^{17}O in N_2O^{60} .

153 Eqn. (10) can be rearranged to give an equation for γ as a function of κ (the full
 154 derivation is presented in Supplementary text S1):

$$\gamma = \frac{{}^{15}\text{R}^\alpha + \kappa {}^{15}\text{R}^\beta + {}^{15}\text{R}^\alpha {}^{15}\text{R}^\beta - ({}^{31}\text{R} - {}^{17}\text{R})[1 + (1 - \kappa) {}^{15}\text{R}^\beta]}{{}^{15}\text{R}^\alpha (1 + {}^{31}\text{R} - {}^{17}\text{R})} \quad (11)$$

155 For two reference materials, we can write two such equations and solve for two
 156 unknowns, γ and κ . ${}^{15}\text{R}^\alpha$ and ${}^{15}\text{R}^\beta$ represent *known* values for each reference material, and ${}^{31}\text{R}$ is
 157 the observed quantity. Essentially, we are asking what values of γ and κ for a pair of known ${}^{15}\text{R}^\alpha$
 158 and ${}^{15}\text{R}^\beta$ values gives the observed ${}^{31}\text{R}$ for each reference gas. Setting the two solutions for γ
 159 equal allows us to determine κ and γ algebraically from the assigned ${}^{15}\text{R}$ values of reference
 160 materials 1 and 2 (${}^{15}\text{R}_1^\alpha$, ${}^{15}\text{R}_1^\beta$, ${}^{15}\text{R}_2^\alpha$, ${}^{15}\text{R}_2^\beta$), their observed ${}^{31}\text{R}$ values (${}^{31}\text{R}_1$, ${}^{31}\text{R}_2$), and the ${}^{17}\text{R}$
 161 values (${}^{17}\text{R}_1$, ${}^{17}\text{R}_2$):

$$\kappa = \frac{\frac{({}^{15}\text{R}_1^\alpha - {}^{31}\text{R}_1 + {}^{17}\text{R}_1)(1 + {}^{15}\text{R}_1^\beta)}{{}^{15}\text{R}_1^\alpha (1 + {}^{31}\text{R}_1 - {}^{17}\text{R}_1)} - \frac{({}^{15}\text{R}_2^\alpha - {}^{31}\text{R}_2 + {}^{17}\text{R}_2)(1 + {}^{15}\text{R}_2^\beta)}{{}^{15}\text{R}_2^\alpha (1 + {}^{31}\text{R}_2 - {}^{17}\text{R}_2)}}{\frac{{}^{15}\text{R}_2^\beta}{{}^{15}\text{R}_2^\alpha} - \frac{{}^{15}\text{R}_1^\beta}{{}^{15}\text{R}_1^\alpha}} \quad (12a)$$

$$\gamma = \frac{\frac{({}^{15}\text{R}_1^\alpha - {}^{31}\text{R}_1 + {}^{17}\text{R}_1)(1 + {}^{15}\text{R}_1^\beta)}{{}^{15}\text{R}_1^\alpha (1 + {}^{31}\text{R}_1 - {}^{17}\text{R}_1)} \left(\frac{{}^{15}\text{R}_2^\beta}{{}^{15}\text{R}_2^\alpha} \right) - \frac{({}^{15}\text{R}_2^\alpha - {}^{31}\text{R}_2 + {}^{17}\text{R}_2)(1 + {}^{15}\text{R}_2^\beta)}{{}^{15}\text{R}_2^\alpha (1 + {}^{31}\text{R}_2 - {}^{17}\text{R}_2)} \left(\frac{{}^{15}\text{R}_1^\beta}{{}^{15}\text{R}_1^\alpha} \right)}{\frac{{}^{15}\text{R}_2^\beta}{{}^{15}\text{R}_2^\alpha} - \frac{{}^{15}\text{R}_1^\beta}{{}^{15}\text{R}_1^\alpha}} \quad (12b)$$

162 After substituting ${}^{45}\text{R} - {}^{15}\text{R}^\alpha - {}^{15}\text{R}^\beta$ for ${}^{17}\text{R}$, the equations for γ and κ can also be written as
 163 follows:

$$\kappa = \frac{\frac{({}^{45}\text{R}_1 - {}^{31}\text{R}_1 - {}^{15}\text{R}_1^\beta)(1 + {}^{15}\text{R}_1^\beta)}{{}^{15}\text{R}_1^\alpha (1 + {}^{15}\text{R}_1^\alpha + {}^{15}\text{R}_1^\beta + {}^{31}\text{R}_1 - {}^{45}\text{R}_1)} - \frac{({}^{45}\text{R}_2 - {}^{31}\text{R}_2 - {}^{15}\text{R}_2^\beta)(1 + {}^{15}\text{R}_2^\beta)}{{}^{15}\text{R}_2^\alpha (1 + {}^{15}\text{R}_2^\alpha + {}^{15}\text{R}_2^\beta + {}^{31}\text{R}_2 - {}^{45}\text{R}_2)}}{\frac{{}^{15}\text{R}_2^\beta}{{}^{15}\text{R}_2^\alpha} - \frac{{}^{15}\text{R}_1^\beta}{{}^{15}\text{R}_1^\alpha}} \quad (13a)$$

$$\gamma = \frac{\frac{(^{45}R_1 - ^{31}R_1 - ^{15}R_1^\beta)(1 + ^{15}R_1^\beta)}{^{15}R_1^\alpha(1 + ^{15}R_1^\alpha + R_1^\beta + ^{31}R_1 - ^{45}R_1)} \left(\frac{^{15}R_2^\beta}{^{15}R_2^\alpha} \right) - \frac{(^{45}R_2 - ^{31}R_2 - ^{15}R_2^\beta)(1 + ^{15}R_2^\beta)}{^{15}R_2^\alpha(1 + ^{15}R_2^\alpha + ^{15}R_2^\beta + ^{31}R_2 - ^{45}R_2)} \left(\frac{^{15}R_1^\beta}{^{15}R_1^\alpha} \right)}{\frac{^{15}R_2^\beta}{^{15}R_2^\alpha} - \frac{^{15}R_1^\beta}{^{15}R_1^\alpha}} \quad (13b)$$

To obtain $^{31}R_1$ and $^{31}R_2$ in continuous-flow analysis, we measure two reference materials (CA08214 and 53504, Table 1) against a common working reference gas (wr), which is calibrated independently (“Lab 1 pure N₂O direct injection” and “Lab 2 pure N₂O direct injection” in Table 1). The working reference is a third calibrated reference material that normalizes different runs to the same reference frame:

$$^{31}R_1 = (1 + ^{31}\delta_1)^{31}R_{wr} \quad (14)$$

$$^{31}R_2 = (1 + ^{31}\delta_2)^{31}R_{wr} \quad (15)$$

where $^{31}R_1$ and $^{31}R_2$ are calculated values that depend on γ and κ , $^{31}\delta$ is the measured ion current ratio difference of sample (1 or 2) to working reference peak, and $^{31}R_{wr}$ is an assumed value calculated with constant γ and κ and assigned $^{15}R^\alpha$, $^{15}R^\beta$, and ^{17}R . Calculating $^{31}R_{wr}$ with constant γ and κ assumes that the working reference peak experiences a defined scrambling behavior that could differ from that of a sample peak; ultimately, however, $^{31}R_{wr}$ drops out of the final $\delta(^{15}\text{N}^{\text{sp}})$ calculation, so this assumption has little effect.

The “algebraic” solution in pyisotopomer⁶⁵ uses $^{31}R_1$ and $^{31}R_2$ in eqns. (11) and (12) to obtain γ and κ . The “least_squares” method in pyisotopomer⁶⁵ solves eqns. (14) and (15) for γ and κ iteratively with a least squares optimization routine. We present a full discussion of the appropriate use of the algebraic and least squares methods in section 4.2.

Some of the isotopomer literature obtains $^{15}R^{\text{bulk}}$ and $^{15}R^\alpha$ by regression between true and measured values of reference materials, inferring $^{15}R^\beta$ indirectly²⁰. In this case, a linear calibration curve replaces the scrambling correction. However, a linear calibration curve just based on “known” $\delta(^{15}\text{N}^\alpha)$ values will fail unless the “known” $\delta(^{15}\text{N}^{\text{sp}})$ values are constant — in other words, a linear calibration curve is only acceptable if the unknowns are close in their $\delta(^{15}\text{N}^{\text{sp}})$ to those of the reference material. It is not accurate if unknowns diverge in their $\delta(^{15}\text{N}^{\text{sp}})$ from that of the reference material(s). This is because the measured $^{31}\delta$ value depends on both $^{15}R^\alpha$ and $^{15}R^\beta$ (Supplementary text S2).

To obtain $^{15}R^\alpha$, $^{15}R^\beta$, and ^{18}R of unknowns, pyisotopomer solves for these values from eqns. (3), (4), (5), and (10), using ^{31}R , ^{45}R , ^{46}R , γ , and κ as input terms⁵⁰. The delta values $\delta(^{15}\text{N}^\alpha)$, $\delta(^{15}\text{N}^\beta)$, $\delta(^{15}\text{N}^{\text{sp}})$, $\delta(^{15}\text{N}^{\text{bulk}})$, and $\delta(^{18}\text{O})$ are calculated from $^{15}R^\alpha$, $^{15}R^\beta$, and ^{18}R relative to primary reference scales (^{15}R from atmospheric N₂, ^{17}R and ^{18}R from VSMOW; if desired, the values of primary reference scale ratios may be adjusted with keyword arguments, as described in the pyisotopomer Documentation⁶⁵). Additionally, if $\Delta^{17}\text{O}$ has been measured separately^{60,62,63}, pyisotopomer can take this value into account in the calculation of $\delta(^{15}\text{N}^\alpha)$, $\delta(^{15}\text{N}^\beta)$, $\delta(^{15}\text{N}^{\text{sp}})$, $\delta(^{15}\text{N}^{\text{bulk}})$, and $\delta(^{18}\text{O})$.

3. Experimental methods

3.1 Preparation and analysis of dissolved N₂O reference materials

A series of dissolved N₂O reference materials (Table 1) were prepared and analyzed in both Lab 1 and Lab 2. Reference materials were prepared by filling 160-mL glass serum bottles (Wheaton) with de-ionized water and removing a 4-mL headspace (Lab 1) or 10 to 20-mL headspace (Lab 2), then capped with a gray butyl rubber septum (National Scientific) and sealed with an aluminum crimp seal. These bottles were purged with helium for 90 minutes at yields a minimum flow rate of 100 mL/min to remove all background N₂O. The purged bottles were then injected with 2 to 43 nmol N₂O to give N₂O concentrations of 13 to 275 nM (Lab 1) or 1 to 60 nmol N₂O to give N₂O concentrations of 6 to 427 nM (Lab 2) in a matrix of He or synthetic air (Table 1) using a gas-tight syringe. Reference materials prepared in Lab 1 were preserved with 100 μ L saturated mercuric chloride (HgCl₂) solution; those prepared in Lab 2 contained no added preservative. For Lab 1, atmosphere-equilibrated seawater was prepared by filtering surface seawater (collected in Half Moon Bay, CA) through a 0.22 mm Sterivex filter, allowing it to undergo static equilibration with outdoor air for three days, then re-filtering into 160-mL serum bottles, removing a 1-mL headspace, and preserving with 100 μ L saturated mercuric chloride solution. For Lab 2, atmosphere-equilibrated reference materials were prepared by purging either de-ionized water or a sodium chloride solution with helium, allowing it to undergo static equilibration with outdoor air for three days, filling into 160-mL serum bottles, and removing a 10-mL headspace. While we were able to correct for these differences in reference material preparation, future intercalibration efforts should aim to prepare reference materials the same way in participating laboratories. In addition, the linearity relationships should be determined from analyzing different amounts of gaseous reference materials, to separate any artifacts due to preparation and extraction of dissolved N₂O reference materials from the abundance linearity of the isotope ratio mass spectrometer itself.

Reference materials were run in the same format as samples to account for any potential fractionation associated with the purge-and-trap system. The magnitude of such fractionation was quantified for Lab 1 by running aliquots of the pure N₂O reference tank in sample format; this test yielded offsets of (0.22 \pm 0.52) ‰ for $\delta(^{15}\text{N}^{\text{bulk}})$ and (0.16 \pm 0.62) ‰ for $\delta(^{18}\text{O})$ vs. the reference tank injection (see Supplementary text S3 for a full discussion of potential fractionation effects in the purge-and-trap system).

The reference gases were calibrated independently by J. Mohn (EMPA; mini-QCLAS aerodyne) or S. Toyoda (Tokyo Tech; IRMS), except for one internal standard used by Lab 1 (B6; Table 1). The $\delta(^{17}\text{O})$ values for each gas were calculated assuming a mass-dependent relationship between ^{17}R and ^{18}R (eqn. 5).

Reference gases and samples were measured on Thermo Finnigan DELTA V Plus isotope ratio mass spectrometers (IRMS; Thermo Fisher Scientific, Waltham, MA) in Labs 1 and 2. Each IRMS had Faraday cups configured to simultaneously measure m/z 30, 31, 44, 45, and 46. The measurements from the Lab 1 DELTA V Plus were made under normal operating conditions, using an ionization energy of 124 eV, accelerating voltage of 3 kV, emission current of 1.50 mA, and box and trap currents of 0.68 and 0.82 mA, respectively. The measurements from the Lab 2 DELTA V Plus were made under normal operating conditions, using an ionization energy of 110 eV, accelerating voltage of 3 kV, emission current of 1.00 mA, and box and trap currents of 0.45 and 0.55 mA, respectively. Reference materials and samples were analyzed on custom purge-and-trap systems coupled to each IRMS, which was run in continuous flow mode⁶⁶ (Table 1). The two systems had slight differences in the purge-and-trap method: in Lab 1, liquid from each sample bottle was transferred under helium pressure to a sparging column to extract the

245 dissolved gases⁶⁷; in Lab 2, each sample was extracted by purging directly from the bottle. The
 246 effects of these differences are discussed further in Results and Discussion.

247

248 3.2 Data corrections

249 3.2.1 Linearity relation

250 The measured ion current ratios 31/30, 45/44, and 46/44 of each sample peak were
 251 divided by those of the working reference peak. This produced three molecular isotope delta
 252 values $^{31}\delta+1$, $^{45}\delta+1$, and $^{46}\delta+1$, where $\delta = R_s/R_{wr} - 1$, with the subscripts “s” and “wr” denoting
 253 sample and working reference, respectively (Figure 1, Step 5).

254 The δ values were corrected for the effect of peak size³³. For Lab 1, this was
 255 accomplished by running six reference materials (reference gases S2, B6, A01, CA06261, 90454,
 256 and 94321; Table 1) in size series ranging from 2-43 nmol N₂O. For Lab 2, three reference
 257 materials (CA06261, 53504, and CA08214) were run in size series ranging from 1-60 nmol N₂O
 258 (Figure 1, Step 6).

259 To obtain a single size correction slope from multiple size series, we used the dummy-
 260 variable method of combining regressions⁶⁸. The dummy variable method is an improvement
 261 over simply averaging each individually calculated slope because it implicitly weighs each size
 262 series by its informativeness, producing a slope that is more likely to reflect the overall linearity
 263 behavior of the instrument⁶⁸. For a given material, each measured $\delta+1$ is a linear function of its
 264 peak area (A) plus an intercept ($\gamma_1 + \gamma_2 D_2 + \gamma_3 D_3$):

$$\delta + 1 = \hat{\beta}A + \gamma_1 + \gamma_2 D_2 + \gamma_3 D_3 \quad (16)$$

265 where $\hat{\beta}$ represents the regression coefficient for a particular peak area (for m/z 31,45, or 46),
 266 obtained by multiple linear regression. The intercept for reference material 1 is γ_1 . D_2 and D_3 are
 267 ‘dummy variables’ to adjust γ_1 by an appropriate intercept for reference material 2 ($\gamma_1 + \gamma_2$) and
 268 reference material 3 ($\gamma_1 + \gamma_3$). Thus, for reference material 1, $D_2 = D_3 = 0$; for reference material
 269 2, $D_2 = 1$ and $D_3 = 0$; for reference material 3, $D_2 = 0$ and $D_3 = 1$. These dummy variables allow
 270 us to obtain one slope for each isotope delta from multiple datasets accounting for differences in
 271 intercept, with each reference material weighted by its spread in the x -axis range. Thus, slopes
 272 $\hat{\beta}_{31}$, $\hat{\beta}_{45}$, and $\hat{\beta}_{46}$ were calculated for $^{31}\delta+1$, $^{45}\delta+1$, and $^{46}\delta+1$, respectively, each using eqn. (16).

273 To normalize measured values of $\delta+1$ to a common peak area, we first calculated the
 274 $(\delta+1)_0$ that would be measured at m/z 44 peak area A_0 :

$$(\delta + 1)_0 = \hat{\beta}(A_0) + \gamma_1 + \gamma_2 D_2 + \gamma_3 D_3 \quad (17)$$

275 Note that $(\delta+1)_0$ is still a function of $\hat{\beta}$, the intercepts γ_1 , γ_2 , γ_3 , and the dummy variables D_2 and
 276 D_3 . To obtain the difference $\delta_0 - \delta$ from the measured m/z 44 peak area A , we subtract eqn. (17)
 277 from eqn. (16), to obtain:

$$(\delta + 1)_0 - (\delta + 1) = \hat{\beta}(A_0 - A)$$

278 In this case, the size-corrected molecular isotope ratio, δ_0 , for each sample with measured δ and
 279 peak area A is given by:

$$(\delta + 1)_0 = \hat{\beta}(A_0 - A) + (\delta + 1) \quad (18)$$

280 Eqn. (18) is simply a function of the slope $\hat{\beta}$, the measured (A) and target (A_0) m/z 44 peak areas,
 281 and the measured δ . Thus, eqn. (18) can be applied across a range of peak areas and δ values to
 282 normalize these δ values to a common peak area. Using this method, we normalized the
 283 measured $^{31}\delta+1$, $^{45}\delta+1$, and $^{46}\delta+1$ of each sample to a peak area (A_0) of 20 Vs (volt seconds),
 284 equivalent to 10 nmol N₂O on the Lab 1 IRMS (Figure 1, Step 7). We note that the linearity

correction estimated here implicitly assumes that samples and reference materials are affected by the same relative blank size.

3.2.2 Scale normalization and calculation of ^{17}R

After applying the linearity correction, a scale normalization was applied to $^{45}\delta$ and $^{46}\delta$ (Figure 1, Step 8). The scale normalization for $^{45}\delta$ and $^{46}\delta$ needs to be carried out before the scrambling correction (which is essentially a scale normalization of $^{31}\delta$); otherwise, the wrong bulk $^{15}N/^{14}N$ and $^{18}O/^{16}O$ ratios are implied. Furthermore, while the γ and κ calculations constrain the differences between $\delta(^{15}N^{\alpha})$ and $\delta(^{15}N^{\beta})$, their absolute values are governed by $\delta(^{15}N^{\text{bulk}})$, necessitating that the “correct”, normalized value of $^{45}\delta$ be input to the scrambling equations. This scale normalization is a replacement for any scale normalization or offset correction to the final output δ values, such as the one-point and two-point offset corrections calculated and applied in Mohn et al. (2014).

A scale normalization was calculated for each run included in the intercalibration exercise. Since assigned values of ^{45}R and ^{46}R for each reference gas were unavailable, assigned ^{45}R and ^{46}R were calculated from assigned $^{15}R^{\alpha}$, $^{15}R^{\beta}$, and ^{18}R and eqns. (3), (4), and (5) (Table 1), assuming $^{17}R_{\text{VSMOW}} = 0.000379969$ and $^{18}R_{\text{VSMOW}} = 0.002005258$. Next, the assigned ^{45}R and ^{46}R for each reference gas were divided by the known ^{45}R and ^{46}R of the direct N_2O reference injection to obtain assigned $^{45}\delta$ and $^{46}\delta$ for each reference material. Then, these assigned $^{45}\delta$ and $^{46}\delta$ values were compared to measured $^{45}\delta$ and $^{46}\delta$ values, and scale normalization coefficients were calculated following the logarithmic scale normalization outlined in Kaiser et al. (2007):

$$\ln(1 + ^{45}\delta^n) = m \ln(1 + ^{45}\delta) + b$$

where $^{45}\delta^n$ is the normalized $^{45}\delta$, “m” is the slope of the regression of $\ln(1 + ^{45}\delta^n)$ vs. $\ln(1 + ^{45}\delta)$, and “b” is the intercept (and likewise for $^{46}\delta$). From this regression, the normalized δ values can be obtained:

$$1 + ^{45}\delta^n = e^{b(1 + ^{45}\delta)^m} \quad (19)$$

For the working reference, the values of $^{45}\delta$ and $^{45}\delta^n$ are equal to zero, so the intercept b should be equal to or very close to zero. The benefit of the logarithmic normalization is that, unlike a linear scale normalization, it is scale-invariant⁶²: essentially, the logarithmic scale normalization does not skew the data towards extremely high or low values, and instead equally weights all data points⁶².

Next, a measured ^{18}R was derived from the scale-normalized ^{45}R and ^{46}R for each sample and reference material (Figure 1, Step 8). The size correction and scale normalization were carried out in the pyisotopomer spreadsheet template; the ^{18}R derivation from the scale-normalized ^{45}R and ^{46}R was the first step accomplished by the pyisotopomer code⁶⁵. Deriving ^{18}R was accomplished by assuming a mass-dependent relationship between ^{17}R and ^{18}R (eqn. 5) and $^{15}R^{\alpha} = ^{15}R^{\beta} = ^{15}R^{\text{bulk}}$. These terms are then substituted into eqns. (3) and (4) to yield:

$$^{45}R = 2^{15}R^{\text{bulk}} + ^{17}R_{\text{VSMOW}} \left(\frac{^{18}R}{^{18}R_{\text{VSMOW}}} \right)^{\beta} (\Delta^{17}O + 1) \quad (20)$$

$$^{46}R = ^{18}R + 2^{15}R^{\text{bulk}} \left[^{17}R_{\text{VSMOW}} \left(\frac{^{18}R}{^{18}R_{\text{VSMOW}}} \right)^{\beta} (\Delta^{17}O + 1) \right] + (^{15}R^{\text{bulk}})^2 \quad (21)$$

Note that the slope β of the mass-dependent relationship between ^{17}R and ^{18}R is an adjustable parameter in the code (default: 0.516), and $\Delta^{17}O$ for each reference material may be

1
2
3 323 entered in the data correction template and subsequently accounted for in this correction (default:
4 324 0 ‰). Eqns. (20) and (21) were then solved for ^{18}R and $^{15}R^{\text{bulk}}$ to obtain an estimated ^{18}R and
5 325 $^{15}R^{\text{bulk}}$ for each sample and reference material, and ^{17}R was calculated from ^{18}R according to eqn.
6 326 (5). The resulting ^{18}R , ^{17}R , and $^{15}R^{\text{bulk}}$ were used in the scrambling calculation. They contain an
7 327 error due to the assumption that $^{15}R^{\alpha} = ^{15}R^{\beta} = ^{15}R^{\text{bulk}}$, although the magnitude of this error should
8 328 be small⁶². Later, the isotopomer calculation solves for $^{15}R^{\alpha}$ and $^{15}R^{\beta}$ separately and thus corrects
9 329 this error.

10 330
11 331 In the intercalibration exercise, values of m and b were calculated from the slopes of
12 332 assigned $^{45}\delta^{\text{a}}$ vs. measured $^{45}\delta$ and assigned $^{46}\delta^{\text{a}}$ vs. measured $^{46}\delta$ from the reference materials in
13 333 each run. These runs took place in February 2021 for Lab 1 and August 2020 and November
14 334 2020 for Lab 2. Combined, the scale normalization and size correction should account for any
15 335 size- or isotope-ratio dependent effects, including those of a blank, linearity, or fractionation in
16 336 the GasBench.

17 337 3.2.3 Calculating $^{31}R_{\text{m}}$ of the direct N_2O reference injection

18 338 We used the same scrambling coefficients for the working reference gas as for the
19 339 samples. We recommend that the user calculates the ^{31}R of the direct reference injection ($^{31}R_{\text{wr}}$ in
20 340 eqns. 14 and 15) with the following sequence of steps: 1) calculate $^{31}R_{\text{wr}}$ from eqn. (10) with
21 341 either $\gamma = \kappa = 0.1$, which reflects commonly reported values^{36,50,54}, or an *a priori* estimate, if
22 342 available (Figure 1, Step 9); 2) use that $^{31}R_{\text{wr}}$ to correct data from two reference materials and
23 343 from those reference materials, obtain γ and κ from eqns. (11) and (12) (Figure 1, Step 10); 3)
24 344 use these updated γ and κ to re-calculate $^{31}R_{\text{wr}}$ from eqn. (10) (Figure 1, Step 11). The input γ and
25 345 κ (used to calculate $^{31}R_{\text{wr}}$) and output γ and κ (calculated from paired reference materials) should
26 346 converge quickly, so one iteration of this process should be sufficient. This value of $^{31}R_{\text{wr}}$ can
27 347 then be used to convert $^{31}\delta$ to $^{31}R_{\text{s}}$. The user should also note that there are likely to be multiple
28 348 pairings of input and output γ and κ that will consistently yield indistinguishable delta values.
29 349

30 350 3.2.4 IRMS scrambling calibration and isotopomer calculation

31 351 The "Scrambling" function of pyisotopomer was used to calculate γ and κ algebraically
32 352 from all possible pairings of reference materials CA08214 and 53504 measured on a given IRMS
33 353 (Lab 1 or Lab 2; Figure 1, Step 13). The reference materials CA08214 and 53504 were chosen
34 354 because of their 113 ‰ $\delta(^{15}\text{N}^{\text{sp}})$ difference (see Results and Discussion for a description of how
35 355 to choose reference material pairings), as well as the range of $\delta(^{15}\text{N}^{\alpha})$, $\delta(^{15}\text{N}^{\beta})$, $\delta(^{15}\text{N}^{\text{bulk}})$, and
36 356 $\delta(^{18}\text{O})$ spanned by the two reference materials, which represent values found typically in
37 357 culture^{52,70} and nature^{26,31}. One-week running averages of γ and κ were calculated to smooth their
38 358 variation and used to obtain position-dependent δ values for unknowns and reference materials
39 359 run as unknowns for quality control (CA06261, S2, B6, and atmosphere-equilibrated seawater),
40 360 using the "Isotopomers" function of pyisotopomer (Figure 1, Step 14).

41 361 For comparison, this exercise was repeated, calculating γ and κ iteratively with the least
42 362 squares optimization (Figure 1, Step 12). The mean algebraic γ and κ from the paired reference
43 363 materials CA08214 and 53504 was used as the initial guess for the least squares solver. In this
44 364 case, reference materials CA08214 and CA06261 were used to calculate the least squares γ and

1
2
3
4 365 κ , because these reference materials are close in their calibrated isotopomer values to natural
5 366 abundance unknowns. As above, γ and κ were combined into a one-week running average; these
6
7 367 running averages of γ and κ for each system were used to obtain position-dependent δ values for
8 368 reference materials and unknowns in the intercalibration exercise (Figure 1, Step 14). The
9 369 analytical precisions of $\delta(^{15}\text{N}^\alpha)$, $\delta(^{15}\text{N}^\beta)$, $\delta(^{15}\text{N}^{\text{sp}})$, $\delta(^{15}\text{N}^{\text{bulk}})$, and $\delta(^{18}\text{O})$ produced by each method
10 370 are presented in the Results and Discussion.

11 371 N_2O amounts were obtained from the m/z 44 peak area and instrument N_2O sensitivity⁶⁷.
12 372 To obtain the conversion factor between peak area and amount of N_2O , the peak areas for
13 373 reference material amounts from 1 to 40 nmol N_2O were recorded. Standard deviations for
14 374 inferred N_2O amounts of replicate unknown samples were 0.07 nmol for Lab 1, and 0.19 nmol
15 375 for Lab 2. All data corrections are described in the README documents associated with
16 376 pyisotopomer on the Python Package Index⁶⁵.
17 377

18 378 3.3 Lake water unknowns

19 379 To validate the scrambling calibration, samples of unknown isotopic composition were
20 380 collected from Lake Lugano, Switzerland in July 2020 and analyzed separately by both Lab 1
21 381 and Lab 2. The samples were collected at depths of 10 and 90 meters, including six replicate
22 382 bottles at each depth. Samples were collected into 160-mL glass serum bottles (Wheaton),
23 383 overflowing each bottle twice, closing bubble-free, and removing liquid to form a 10-mL
24 384 headspace comprised of air. Based on the northern hemisphere monthly mean tropospheric N_2O
25 385 mole fraction when the samples were collected in July, 2020⁷¹, an atmospheric headspace of this
26 386 volume would have contained 0.13 nmol N_2O . For Lab 2, where the full amount of N_2O in the
27 387 sample is measured, incorporation of the headspace into the measurement results in a 0.13 nmol
28 388 overestimation of the amount of N_2O in the sample⁷¹. For Lab 1, where 2 mL sample liquid is
29 389 left behind post-analysis, equilibration the 10-mL headspace during sample storage results in
30 390 either an underestimate (0.12 nmol) or overestimate (0.10 nmol) of N_2O in the sample,
31 391 depending on its concentration. In both cases, these errors are similar to the analytical precision
32 392 of the N_2O amount measurement. Each sample was capped with a gray butyl septum (National
33 393 Scientific) and sealed with an aluminum crimp seal. Samples were promptly preserved with 100
34 394 μL saturated mercuric chloride solution and stored at lab temperature (20-22°C). The isotope
35 395 fractionation associated with N_2O partitioning, defined as the isotope ratio of the gas phase
36 396 divided by the isotope ratio of the liquid phase, ($^{15}\epsilon = -0.7\text{‰}$, $^{18}\epsilon = -1.1\text{‰}$, 298.2 K) falls
37 397 within the analytical uncertainty⁷². The six replicate bottles at each depth were split into two
38 398 groups of three replicate bottles to be measured by Lab 1 and Lab 2, respectively.
39 399

40 400 4. Results and Discussion

41 401 4.1 Linearity relation

42 402 Linearity relations were calculated using the dummy variable method described in
43 403 Section 3.2.1 and applied to the intercalibration data as follows. A linearity relation was
44 404 determined for Lab 1 in February 2021 (Figure 2a-c) and applied to lake water samples run in
45 405 Lab 1 and reference materials prepared and run in Lab 1. Reference materials prepared in Lab 2
46 406 but run in Lab 1 exhibited statistically distinct linearity slopes from those both prepared and run
47 407 in Lab 1; thus, a separate linearity relation was applied to these reference materials (but not to the
48 408 lake water samples) (Figure 2d-f). A linearity relation was determined for Lab 2 in May 2020
49 409

(Figure 2g-i) and applied to lake water samples and reference materials run in Lab 2. As previously observed⁷³, for each linearity relation, the slopes of the fits for individual reference materials were identical within error. The linearity correction reduced the spread of measured molecular isotope ratios across size series of each given reference material (Figure S2).

4.2 IRMS scrambling calibration

For both labs, the “algebraic” solution produced reasonable values of γ and κ (i.e., between 0 and 1) for reference material pairings involving the reference material 53504 ($\delta(^{15}\text{N}^{\text{sp}}) = -93\text{‰}$). The mean γ and κ calculated for Lab 1 from reference materials 53504 and CA08214 were 0.174 ± 0.022 and 0.083 ± 0.022 , respectively (Table S2). In August 2020, the mean γ and κ calculated for Lab 2 from the same two reference materials were 0.095 ± 0.011 and 0.091 ± 0.010 , respectively (Table S2). In November 2020, γ and κ for Lab 2 were slightly different but within 1σ of the values measured in August 2020 (0.091 ± 0.013 and 0.086 ± 0.013 , respectively; Table S2). Other reference materials paired with 53504 produced similar values of γ and κ . The difference $\gamma - \kappa$ was also consistent for reference material pairings with 53504: for Lab 1, $\gamma - \kappa$ was 0.090 - 0.091 , and for Lab 2, it was 0.003 - 0.005 (Table S2).

For pairings with 53504, the $\delta(^{15}\text{N}^{\text{sp}})$ difference between both reference materials was greater than 100‰ . Pairs of reference materials with smaller $\delta(^{15}\text{N}^{\text{sp}})$ differences produced more variable γ and κ values with the algebraic solution, which sometimes fell outside the physically plausible range between 0 and 1. For example, in Lab 1, the pairing of CA06261 and CA08214 produced γ and κ values of 0.01 ± 0.23 and -0.08 ± 0.23 , respectively. In this case, the measurement uncertainty was too large — and the $\delta(^{15}\text{N}^{\text{sp}})$ values too close — for the scrambling coefficients to be adequately determined. What matters, however, is that the difference between γ and κ is accurate; as the results show, the absolute values are less important (and can even be negative, greater than 1, or otherwise “unphysical”).

To understand the uncertainty in γ and κ calculated from equations 11 and 12, we define a variable d , which allows us to express the analytical solution for γ and κ (eqns. 13a and 13b) in terms of $\delta(^{15}\text{N}^{\text{sp}})$, $\delta(^{15}\text{N}^{\text{atm}})$, and $\delta(^{15}\text{N}^{\text{sp}})$:

$$d = \frac{(^{15}\text{R}^{\beta} + ^{31}\text{R} - ^{45}\text{R})(1 + ^{15}\text{R}^{\beta})}{^{15}\text{R}_{\text{atm}}(1 + ^{15}\text{R}^{\alpha} + ^{15}\text{R}^{\beta} + ^{31}\text{R} - ^{45}\text{R})} \quad (22)$$

The value of d is similar for all samples and reference gases run on a given IRMS and depends primarily on the difference $^{31}\text{R} - ^{45}\text{R}$. Using δ notation, i.e., $\delta(^{15}\text{N}) = ^{15}\text{R}/^{15}\text{R}_{\text{atm}} - 1$, and dropping the label “ ^{15}N ” for brevity, eqns. (13a) and (13b) can be written as follows:

$$\kappa = \frac{\frac{d_2}{1 + \delta_2^{\alpha}} - \frac{d_1}{1 + \delta_1^{\alpha}}}{\frac{d_2}{1 + \delta_2^{\beta}} - \frac{d_1}{1 + \delta_1^{\beta}}} = \frac{\frac{d_2}{1 + \delta_2^{\alpha}} - \frac{d_1}{1 + \delta_1^{\alpha}}}{\frac{\delta_1^{\text{sp}}}{1 + \delta_1^{\alpha}} - \frac{\delta_2^{\text{sp}}}{1 + \delta_2^{\alpha}}} \quad (23a)$$

$$\begin{aligned}
 \gamma &= \frac{\frac{d_2}{1 + \delta_2^\alpha} \left(\frac{1 + \delta_1^\beta}{1 + \delta_1^\alpha} \right) - \frac{d_1}{1 + \delta_1^\alpha} \left(\frac{1 + \delta_2^\beta}{1 + \delta_2^\alpha} \right)}{\frac{1 + \delta_2^\beta}{1 + \delta_2^\alpha} - \frac{1 + \delta_1^\beta}{1 + \delta_1^\alpha}} \\
 &= \frac{\frac{d_2}{1 + \delta_2^\alpha} \left(\frac{1 + \delta_1^\beta}{1 + \delta_1^\alpha} \right) - \frac{d_1}{1 + \delta_1^\alpha} \left(\frac{1 + \delta_2^\beta}{1 + \delta_2^\alpha} \right)}{\frac{\delta_1^{\beta p}}{1 + \delta_1^\alpha} - \frac{\delta_2^{\beta p}}{1 + \delta_2^\alpha}} \quad (23b)
 \end{aligned}$$

442 The denominators of these expressions can be approximated by the difference $\delta_1^{\beta p} - \delta_2^{\beta p}$.
 443 Thus, if the site preferences of the reference gases are similar, the value of the denominator
 444 approaches zero and the solutions will become uncertain due to the finite measurement error.
 445 Then, the question arises, how far apart must the site preferences of the reference materials be to
 446 obtain robust solutions?

447 The general form of uncertainty propagation in a variable a with respect to the
 448 observations (y_i) is given by the following equation⁷⁴:

$$\sigma_a^2 = \sum_i \sigma_i^2 \left(\frac{\partial a}{\partial y_i} \right)^2$$

450 where σ_a is the uncertainty in a , y_i is an individual observation, and σ_i is the uncertainty in the
 451 observation y_i . Ignoring the uncertainties in ^{45}R and the assigned position-dependent ^{15}R values,
 452 the uncertainty in κ can be calculated as:

$$\sigma_\kappa^2 = \sigma_{^{31}R_1}^2 \left(\frac{\partial \kappa}{\partial ^{31}R_1} \right)^2 + \sigma_{^{31}R_2}^2 \left(\frac{\partial \kappa}{\partial ^{31}R_2} \right)^2$$

$$\begin{aligned}
 \frac{\partial \kappa}{\partial ^{31}R_1} &= \frac{\frac{-(1 + ^{15}R_1^\alpha)(1 + ^{15}R_1^\beta)}{^{15}R_1^\alpha(1 + ^{15}R_1^\alpha + R_1^\beta + ^{31}R_1 - ^{45}R_1)^2} - 1}{\frac{\delta_1^{\beta p}}{1 + \delta_1^\alpha} - \frac{\delta_2^{\beta p}}{1 + \delta_2^\alpha}} \approx \frac{-1}{^{15}R_1^\alpha(\delta_1^{\beta p} - \delta_2^{\beta p})} \\
 \frac{\partial \kappa}{\partial ^{31}R_2} &= \frac{\frac{-(1 + ^{15}R_2^\alpha)(1 + ^{15}R_2^\beta)}{^{15}R_2^\alpha(1 + ^{15}R_2^\alpha + R_2^\beta + ^{31}R_2 - ^{45}R_2)^2} - 1}{\frac{\delta_1^{\beta p}}{1 + \delta_1^\alpha} - \frac{\delta_2^{\beta p}}{1 + \delta_2^\alpha}} \approx \frac{-1}{^{15}R_2^\alpha(\delta_1^{\beta p} - \delta_2^{\beta p})}
 \end{aligned}$$

457 Assuming $\sigma_{^{31}R}/^{15}R^\alpha = \sigma_{^{31}R_1}/^{15}R_1^\alpha = \sigma_{^{31}R_2}/^{15}R_2^\alpha$, then

$$\sigma_{\kappa}^2 \approx 2 \left(\frac{\sigma^{31R}}{^{15}R^{\alpha}} \right)^2 \left(\frac{1}{\delta_1^{\text{sp}} - \delta_2^{\text{sp}}} \right)^2$$

460 or

$$\sigma_{\kappa} \approx \sqrt{2} \frac{\sigma^{(31R)} \quad 1}{^{15}R^{\alpha} \quad |\delta_1^{\text{sp}} - \delta_2^{\text{sp}}|} \quad (24a)$$

461 Similarly, for γ :

$$\sigma_{\gamma} \approx \sqrt{2} \frac{\sigma^{(31R)} \quad 1}{^{15}R^{\beta} \quad |\delta_1^{\text{sp}} - \delta_2^{\text{sp}}|} \quad (24b)$$

462 where $\sigma^{(31R)}/^{15}R$ can be approximated by the measurement uncertainty in $^{31}\delta$ and
 463 $|\delta_1^{\text{sp}} - \delta_2^{\text{sp}}|$ is the absolute value of the difference in assigned site preferences between the two
 464 reference materials. This means that for a measurement uncertainty in $^{31}\delta$ of 1 ‰ and a $\delta(^{15}\text{N}^{\text{sp}})$
 465 difference of 10 ‰ between the two reference materials, γ and κ would have absolute
 466 uncertainties of 0.14. This uncertainty translates into a relative uncertainty of about 30 % for the
 467 $\delta(^{15}\text{N}^{\text{sp}})$ value of an unknown sample – far too high for practical applications (Supplementary
 468 text S4). A $\delta(^{15}\text{N}^{\text{sp}})$ difference of 100 ‰ would give a more useful absolute uncertainty of 0.014
 469 for γ and κ .

470 These theoretical uncertainties are reflected in the experimental data. For Lab 1, the
 471 reference materials 53504 ($\delta(^{15}\text{N}^{\text{sp}}) = -92.73$ ‰) and CA08214 ($\delta(^{15}\text{N}^{\text{sp}}) = 20.54$ ‰) yielded $\gamma =$
 472 0.174 ± 0.022 and $\kappa = 0.083 \pm 0.022$. The standard deviation of $^{31}\delta$ was 1.89 ‰ ($n = 12$). This
 473 produces an estimated uncertainty in γ and κ of $\sqrt{2}(1.89 \text{ ‰})/(113.27 \text{ ‰}) = 0.024$, which agrees
 474 well with the experimental data. Similarly, reference materials 53504 and CA06261 ($\delta(^{15}\text{N}^{\text{sp}}) =$
 475 27.07 ‰) yielded $\gamma = 0.163 \pm 0.018$ and $\kappa = 0.073 \pm 0.018$. The standard deviation of $^{31}\delta$ was 1.58
 476 ‰ ($n = 10$), and the $\delta(^{15}\text{N}^{\text{sp}})$ difference was 119.80 ‰. This produced an estimated uncertainty in
 477 γ and κ of $\sqrt{2}(1.58 \text{ ‰})/(119.80 \text{ ‰}) = 0.019$, also in line with the uncertainties in γ and κ .

478 Rearranging eqns. (24a) and (24b), we obtain expressions for the required $|\delta_1^{\text{sp}} - \delta_2^{\text{sp}}|$ to
 479 obtain a target level of uncertainty (σ) in γ and κ , given the measurement uncertainty in ^{31}R :

$$|\delta_1^{\text{sp}} - \delta_2^{\text{sp}}| = \sqrt{2} \frac{\sigma^{(31R)} \quad 1}{^{15}R^{\alpha} \quad \sigma_{\kappa}} \quad (25a)$$

$$|\delta_1^{\text{sp}} - \delta_2^{\text{sp}}| = \sqrt{2} \frac{\sigma^{(31R)} \quad 1}{^{15}R^{\beta} \quad \sigma_{\gamma}} \quad (25b)$$

481 Assuming $\sigma^{(31R)}/^{15}R^{\alpha} \approx \sigma^{(31R)}/^{15}R^{\beta} \approx \sigma(^{31}\delta)$, we obtain:

$$|\delta_1^{\text{sp}} - \delta_2^{\text{sp}}| = \sqrt{2} \sigma(^{31}\delta) \frac{1}{\sigma_{\gamma\kappa}} \quad (26)$$

483 where $\sigma(^{31}\delta)$ is the $^{31}\delta$ measurement uncertainty in per mil, and $\sigma_{\gamma\kappa}$ is the target absolute
 484 uncertainty in γ and κ . For example, with a measurement uncertainty of 1 ‰ in $^{31}\delta$, the $\delta(^{15}\text{N}^{\text{sp}})$
 485 values of the two reference materials must differ by at least 141 ‰ to achieve an absolute
 486 uncertainty in γ and κ of 0.01. Based on these results, we recommend calculating γ and κ from
 487 reference materials with a large $\delta(^{15}\text{N}^{\text{sp}})$ difference, as estimated from eqn. (26).

488 As an alternative to the algebraic solution, a least squares optimization can be used to
 489 find a solution for γ and κ , although that solution may find a local optimum rather than a global
 490 optimum. The user can select a least squares optimization instead of the algebraic solution with
 491 the “method” keyword argument to pyisotopomer’s Scrambling function. The least squares
 492 optimization smooths measurement uncertainty, making it useful for fitting repeat
 493 measurements of reference materials to a single pair of “best” values for γ and κ . Its disadvantage
 494 is that, unlike the algebraic solution, the least squares optimization depends on the initial guess
 495 for γ and κ . Using data from reference materials CA06261 and CA08214, a range of initial
 496 guesses from $\gamma = \kappa = 0.000$ to $\gamma = \kappa = 0.200$ produced a range of least squares solutions, from $\gamma =$
 497 0.090 and $\kappa = 0.000$ to $\gamma = 0.269$ and $\kappa = 0.183$ (Figure S3). Despite this range of γ and κ ,
 498 however, the least squares optimization produced a consistent $\gamma - \kappa$ of 0.09. As shown in Section
 499 4.4, $\gamma - \kappa$ governs the accuracy of $\delta(^{15}\text{N}^{\text{sp}})$ far more than the individual values of γ and κ .

500 Given an accurate initial guess, the least squares optimization will find a minimum at or
 501 close to this initial guess, even for reference material pairings close in their $\delta(^{15}\text{N}^{\text{sp}})$. For
 502 example, when we used the algebraic γ and κ from reference materials CA08214 and 53504 as an
 503 initial guess, the least squares optimization produced similar γ and κ for a variety of reference
 504 material pairings (Table S2). Furthermore, for the same initial guess, the least squares
 505 optimization finds different solutions for the Lab 1 and Lab 2 instruments, even for reference
 506 material pairings close in their $\delta(^{15}\text{N}^{\text{sp}})$ (Table S3). This demonstrates that, depending on the
 507 measurement precision at the time, the least squares optimization searches an appropriately wide
 508 solution space to resolve large differences in instrument behavior.

509 If the first-time user wishes to obtain accurate individual values of γ and κ , we
 510 recommend obtaining reference materials different enough in their $\delta(^{15}\text{N}^{\text{sp}})$ to calculate γ and κ
 511 with the algebraic solution. If the user wishes to take advantage of the smoothing of the least
 512 squares optimization, this algebraic γ and κ can then be used as the initial guess for the least
 513 squares solver.

514 We also recommend that the user test the accuracy of the least squares γ and κ by
 515 plugging γ and κ back into eqn. (10) and comparing the result to the measured ^{31}R for each
 516 reference material. The two ^{31}R values should match. pyisotopomer⁶⁵ performs this calculation
 517 automatically and outputs the difference as a δ value:

$$^{31}\delta_{\text{error}} = \frac{^{31}R_{\text{calculated}}}{^{31}R_{\text{measured}}} - 1 \quad (27)$$

518

1
2
3
4 519 where ${}^{31}R_{\text{calculated}}$ is calculated by plugging the least squares γ and κ into eqn. (10), and
5 520 ${}^{31}R_{\text{measured}}$ represents the measured ${}^{31}R$ for each reference material. In the intercalibration
6 521 exercise, the mean of the absolute values of ${}^{31}\delta^{\text{error}}$ from least squares γ and κ solutions ranged
7 522 from 0.27 ‰ to 0.86 ‰ (Table S2), similar in magnitude to the ${}^{31}\delta$ analytical uncertainty for
8 523 Labs 1 and 2 (Table S5). This indicates that the amount of error introduced by using the least
9 524 squares optimization is similar to the measurement error in ${}^{31}\delta$ (Table S2, Table S5). In
10 525 comparison, the ${}^{31}\delta^{\text{error}}$ introduced by the algebraic solution corresponded to values of $({}^{31}R_{\text{calculated}}$
11 526 $- {}^{31}R_{\text{measured}})$ within machine precision (Table S2).
12
13 527

14 528 4.3 Variability in fragmentation behavior

15
16 529 As shown above, $\gamma - \kappa$, as opposed to the individual values of γ and κ , is the best
17
18 530 constrained parameter in the scrambling calculation. We show below that $\gamma - \kappa$ also has the
19
20 531 greatest impact on $\delta({}^{15}\text{N}^{\alpha})$, $\delta({}^{15}\text{N}^{\beta})$, and $\delta({}^{15}\text{N}^{\text{sp}})$. $\gamma - \kappa$ is proportional to ${}^{31}\delta - {}^{45}\delta$, and thus is a
21 532 metric of an instrument's scrambling behavior.

22 533 To examine the change in the fragmentation behavior of a single IRMS over time, we
23
24 534 compiled values of $\gamma - \kappa$ for Lab 1 from June 2018 – March 2021 (Figure 3). To equally weigh
25 535 each day of running the instrument, first, we calculated a daily mean $\gamma - \kappa$, then calculated a five-
26
27 536 day running average of $\gamma - \kappa$ from these daily means. The value of $\gamma - \kappa$ varied throughout the
28
29 537 time series, with a mean of 0.092 ± 0.002 . High volatility in $\gamma - \kappa$ in February-April 2019
30 538 corresponded with a period when the lab temperature was poorly controlled, with strong day-
31 539 night variation (Figure 3). During periods when the lab temperature was stable, $\gamma - \kappa$ tended to
32 540 increase as the instrument box and trap currents diverged with filament age, although no linear
33 541 relationship emerged.

34
35 542 There are several reasons why the scrambling behavior of the ion source might change
36 543 over time, as well as differing between instruments. The NO^+ fragment ion can be produced by
37 544 one of several routes from N_2O^+ ^{75,76}. The pathways and associated isotope effects for the
38 545 formation of fragment ions are affected by collision frequency, the distribution of excited states,
39 546 and the time spent in the ion source, which suggests that ion source conditions such as vapor
40 547 pressure, ionizing energy, and accelerating voltage may all influence the fragmentation behavior
41 548 of an IRMS system^{54,75-78}. Future work could track the effect of variation in these parameters on
42 549 the fragmentation behavior of the instrument, as in Westley et al.⁵⁴, which may allow for
43 550 optimization of fragmentation and scrambling in the ion source.

44 551 For these reasons, performing the scrambling calibration only once is insufficient to
45
46 552 obtain high-quality N_2O isotopocule data. Instead, it is important to recalibrate an IRMS system
47 553 for scrambling on a regular basis since ion source conditions may change with time and can shift
48 554 abruptly with events such as filament changes. We recommend using a running average of γ and
49
50 555 κ over a window corresponding to 10 pairings of reference materials, corresponding to a five-day
51
52 556 window if two pairs of reference materials are run per day. If there is high volatility in γ and κ , as
53 557 seen above in March-April 2019, it may be necessary to shorten this window, to apply
54 558 scrambling corrections most appropriate to instrument conditions.
55 559

4.4 Sensitivity of position-dependent δ values to uncertainty in scrambling coefficients

The uncertainty in $\delta(^{15}\text{N}^\alpha)$, $\delta(^{15}\text{N}^\beta)$, and $\delta(^{15}\text{N}^{\text{sp}})$ associated with the uncertainty in each scrambling coefficient is less straightforward to assess than the uncertainty in ^{31}R given by eqns. (23) and (24), due to the nonlinear relationship between $\delta(^{15}\text{N}^\alpha)$, $\delta(^{15}\text{N}^\beta)$, γ , and κ . (see eqn. (53) of Kaiser and Röckmann, 2008). A first order approximation of $\delta(^{15}\text{N}^{\text{sp}})$ is given by (supplementary text S4):

$$\delta(^{15}\text{N}^{\text{sp}}) \approx \frac{2(1 - \gamma + \kappa)}{1 - \gamma - \kappa} ({}^{31}\delta - {}^{45}\delta) \quad (28)$$

From this equation, it is apparent that $\delta(^{15}\text{N}^{\text{sp}})$ is modulated primarily by the difference $\gamma - \kappa$, rather than the individual values of γ and κ . It is also apparent that $\gamma - \kappa$ is proportional to ${}^{31}\delta - {}^{45}\delta$.

A Monte Carlo simulation can be a useful way of visualizing how γ , κ , and $\gamma - \kappa$ impact $\delta(^{15}\text{N}^\alpha)$, $\delta(^{15}\text{N}^\beta)$, and $\delta(^{15}\text{N}^{\text{sp}})$. We performed two sensitivity experiments with data from Lab 1:

- 1) sensitivity of $\delta(^{15}\text{N}^\alpha)$, $\delta(^{15}\text{N}^\beta)$, and $\delta(^{15}\text{N}^{\text{sp}})$ to $\gamma - \kappa$;
- 2) sensitivity of $\delta(^{15}\text{N}^\alpha)$, $\delta(^{15}\text{N}^\beta)$, and $\delta(^{15}\text{N}^{\text{sp}})$ to the individual values of γ and κ , holding their difference constant.

For the first sensitivity experiment, a Monte Carlo simulation was used to introduce random uncertainty in the γ and κ values used to calculate δ values of three reference materials. Based on Table S2, we chose $\gamma = 0.174$ and $\kappa = 0.083$ as central values and varied $\gamma - \kappa$ such that the standard deviation of $\gamma - \kappa$ was equal to 10 % of the mean (0.091). For the second sensitivity experiment, we modeled γ and κ in tandem as random numbers centered around $\gamma = 0.174$ and $\kappa = 0.083$, with uncertainties equal to 10 % of the mean γ , and held $\gamma - \kappa$ constant at 0.091. For both experiments, we sampled 1000 pairs of γ and κ , and then calculated the 1000 simulated values of $\delta(^{15}\text{N}^\alpha)$, $\delta(^{15}\text{N}^\beta)$, and $\delta(^{15}\text{N}^{\text{sp}})$ for the three reference materials (CA06261, 53504, CA08214).

This analysis showed that a 10 % relative uncertainty in $\gamma - \kappa$ can lead to large variations in $\delta(^{15}\text{N}^\alpha)$, $\delta(^{15}\text{N}^\beta)$, and $\delta(^{15}\text{N}^{\text{sp}})$, e.g., pooled standard deviations of 17.1-18.5 ‰ for $\delta(^{15}\text{N}^{\text{sp}})$ (Figure 4a-c). In contrast, a 10 % relative error in γ , keeping $\gamma - \kappa$ constant, led to pooled standard deviations of 1.0-4.3 ‰ in $\delta(^{15}\text{N}^{\text{sp}})$ (Figure 4d-f). In both experiments, varying γ and κ produced the most variability for reference material 53504, whose $\delta(^{15}\text{N}^{\text{sp}})$ was greatest in magnitude.

These results reflect the earlier conclusion that $\gamma - \kappa$ is the best constrained parameter in the scrambling calculation, and, conversely, that this difference has the greatest effect on $\delta(^{15}\text{N}^{\text{sp}})$. Thus, we recommend regular scrambling calibrations, as assuming the wrong $\gamma - \kappa$ difference may have a significant impact on site preferences calculated from these coefficients.

4.5 Comparison of results between two IRMS laboratories

The application of pyisotopomer was tested through an intercalibration including four reference materials and two Lake Lugano samples measured by two IRMS laboratories, plus two additional reference materials run in Lab 1. Using an average γ and κ produced by the algebraic

method from the pairing of reference materials 53504 and CA08214, isotopomers were calculated for lake water unknowns, four reference materials run as unknowns for quality control, and the two reference materials used in the calibration and (Table 2). This exercise was repeated, calculating γ and κ instead with least squares method and the pairing of reference materials CA06261 and CA08214 (Table S4). The root mean square deviation (RMSD) for each reference material was calculated by comparison to the calibrated values provided by a previous intercalibration effort⁵⁶ (for atmosphere-equilibrated seawater), an internal standard (B6), and four gases sourced from J. Mohn (S2, CA06261, 53504, and CA08214). Almost all isotopomer values produced by the least squares optimization (Table S4) were within error of those produced by the algebraic solution (Table 2); the latter is discussed below.

The $\delta(^{15}\text{N}^{\text{bulk}})$ measured by the two labs displayed good agreement for each of the four reference materials, as well as the lake water samples. The $\delta(^{15}\text{N}^{\text{bulk}})$ RMSDs ranged from 0.2 to 0.6 ‰ (Table 2), all of which were smaller than the 0.8 ‰ presented for IRMS labs by Mohn et al., (2014). The RMSD for atmospheric N_2O was highest, at 0.6 ‰. For both lake water samples, the $\delta(^{15}\text{N}^{\text{bulk}})$ values measured by Lab 1 and Lab 2 were statistically indistinguishable (Table 2; Figure S4). Likewise, the $\delta(^{18}\text{O})$ measured by the two labs displayed good agreement for each of the four reference materials measured by both labs, as well as the lake water samples. The $\delta(^{18}\text{O})$ RMSDs were slightly greater than the 1.00 ‰ presented for IRMS labs by Mohn et al. (2014), ranging from 0.5 ‰–1.7 ‰, with the greatest RMSD for reference material 53504 (Table 2). For the lake water unknowns, the $\delta(^{18}\text{O})$ values measured by the two labs were within error of each other (Table 2; Figure S4).

The $\delta(^{15}\text{N}^{\alpha})$ measured by the two labs also showed good agreement for reference materials CA06261, CA08214, and atmosphere-equilibrated seawater: in each case, the combined RMSD was less than 2.4 ‰ (Table 2). This is similar to the data presented in Mohn et al. (2014), who find an RMSD for $\delta(^{15}\text{N}^{\alpha})$ for IRMS laboratories of 2.47 ‰. The $\delta(^{15}\text{N}^{\alpha})$ measured by Lab 1 for reference material 53504 (0.0 ± 1.0 ‰) was lower than both the calibrated value (1.71 ‰) and the value measured by Lab 2 (1.7 ± 1.0 ‰). The values of $\delta(^{15}\text{N}^{\alpha})$ measured by the two labs for the two lake water samples, however, were within error of each other. For $\delta(^{15}\text{N}^{\beta})$, the RMSDs for each reference material were of a similar order of magnitude to $\delta(^{15}\text{N}^{\alpha})$, ranging from 0.2 ‰–2.1 ‰, similar to the value 2.12 ‰ reported by Mohn et al. (2014). The $\delta(^{15}\text{N}^{\beta})$ measured by Lab 1 for the lake water unknowns was within error of that measured by Lab 2 (Table 2; Figure S4). Of note, the $\delta(^{15}\text{N}^{\beta})$ for the lake water unknown taken at 90 m depth was -32.8 ‰ (average of measurements by Lab 1 and Lab 2), which is far more negative than most values observed previously^{26,31}.

The $\delta(^{15}\text{N}^{\text{sp}})$ values measured by the two laboratories showed larger standard deviations than the $\delta(^{15}\text{N}^{\alpha})$ and $\delta(^{15}\text{N}^{\beta})$ individually, which is to be expected, since $\delta(^{15}\text{N}^{\text{sp}})$ is a measure of difference between the latter two parameters. The $\delta(^{15}\text{N}^{\text{sp}})$ RMSD values, however, were all less than 3 ‰ for atmosphere-equilibrated seawater, 53504, and CA08214 (Table 2). This represents an improvement on Mohn et al. (2014), who find an RMSD of 4.29 ‰ for $\delta(^{15}\text{N}^{\text{sp}})$ measured by IRMS laboratories. The $\delta(^{15}\text{N}^{\text{sp}})$ RMSD for reference material CA06261 was greater, at 4.4 ‰, which may result from this reference material having a more negative $\delta(^{15}\text{N}^{\alpha})$ than either of the two reference materials used in the scrambling calibration. The lake water samples showed larger offsets in $\delta(^{15}\text{N}^{\text{sp}})$ than the reference materials (Figure S4). The lake water sample from 10 m depth showed an especially large difference in $\delta(^{15}\text{N}^{\text{sp}})$ between Lab 1 and Lab 2: Lab 1 measured a mean $\delta(^{15}\text{N}^{\text{sp}})$ of (18.8 ± 1.6) ‰ at this depth, while Lab 2 measured a mean $\delta(^{15}\text{N}^{\text{sp}})$

of (21.4±2.5) ‰ (Table 2). At 90 m depth, Lab 1 measured a mean $\delta(^{15}\text{N}^{\text{sp}})$ of 52.3±1.2 ‰, and Lab 2 measured a mean $\delta(^{15}\text{N}^{\text{sp}})$ of (50.9±0.5) ‰.

After size correction and scale normalization, the only consistent difference between measurements made by the two labs were differences in peak area, which may reflect differences in the setup of the purge and trap system and/or differences in instrument sensitivity. The N_2O amounts (in nmol) measured in the lake water samples were also similar between the two labs involved in the intercalibration exercise, indicating that this difference in sensitivity was adequately compensated for by the peak area to amount conversion factor. In the sample taken at 10 m depth, Lab 1 found (2.97±0.04) nmol; Lab 2 found (2.31±0.09) nmol. At 90 m depth, Lab 1 found (20.46±0.37) nmol; Lab 2 found (19.82±0.01) nmol N_2O . The intercalibration is expressed in terms of N_2O amounts instead of concentrations to eliminate uncertainties in sample volume; all bottle volumes were the same. Thus, we conclude that differences in sample pretreatment procedure were corrected for by the size correction and scale normalization steps, leaving no residual effect on the final δ values or N_2O amounts.

4.6 Additional considerations

The pyisotopomer package produces good results if each of the data preprocessing steps properly account for size- and delta-dependent effects on the measured isotope ratios $^{31}\delta$, $^{45}\delta$, and $^{46}\delta$. However, it will produce spurious results under the following circumstances. Firstly, varying blanks may introduce errors due to the size correction not being applicable to samples and reference materials alike. Second, if the $^{45}\delta$ and $^{46}\delta$ scale normalization slope and intercept differ substantially from one and zero (such as a negative slope), there likely exists an issue with the scale normalization (such as the reference materials not spanning a wide enough range in $^{45}\delta$ and $^{46}\delta$). A spurious scale normalization will likewise produce errors in the final isotopocule values. Thirdly, if reference materials that are too close in their site preferences are used to determine γ and κ with the algebraic solution, the resulting coefficients may represent "unphysical" values (i.e., not between 0 and 1); these, however, would be inconsequential if the unknown samples have $\delta(^{15}\text{N}^{\text{sp}})$ values close to these reference materials. Finally, $\delta(^{17}\text{O})$ is calculated from a mass dependent relationship with $\delta(^{18}\text{O})$ (the parameters of which can be adjusted with keyword arguments to the Scrambling and Isotopomers functions) unless $\Delta(^{17}\text{O})$ is determined separately^{60,62,63} and entered in the data corrections template.

5. Conclusion: How to obtain high-quality N_2O isotopocule data using pyisotopomer

Using pyisotopomer and three reference materials, one can characterize the scrambling behavior for a given IRMS and apply those scrambling coefficients to calculate the isotopocule values of unknown samples. To ensure high-quality results from these calculations, we provide the following recommendations. Firstly, if reference materials with suitably distinct site preferences are available, we recommend calculating the scrambling coefficients γ and κ from algebraic solution of eqns. (11) and (12), which is the default method in the Scrambling function of pyisotopomer. We offer the least squares approach as an alternative, with the following caveats: 1) The least squares solver finds a minimum close to the initial guess for γ and κ . As such, if the solver is fed an initial guess other than the absolute minimum calculated from the algebraic solution, it will find the "wrong" absolute value of γ and κ . It will, however, find the correct value of $\gamma - \kappa$, which has a much larger impact on calculated isotopocules. 2) Using the

1
2
3 686 “wrong” scrambling coefficients will have only a small effect if the unknowns are close in their
4 687 $\delta(^{15}\text{N}^\alpha)$, $\delta(^{15}\text{N}^\beta)$, and $\delta(^{15}\text{N}^{\text{sp}})$ to those of the reference materials but will have a deleterious effect
5 688 as the unknowns diverge in their isotopomer values from the reference materials. 3) If an initial
6 689 guess is available, such as through a calibration with the algebraic solution, this should be used
7 690 as the initial guess for the least squares solver. Otherwise, we recommend iterating through the
8 691 scrambling calculation twice, using the solution from the first iteration as the initial guess for
9 692 subsequent calculations. It is necessary to run paired reference materials daily to obtain accurate
10
11 693 running estimates of γ and κ . It is recommended to convert these daily estimates to a one-week
12 694 running average and use that average to calculate the isotopocules of unknown samples.

13 695 Using pyisotopomer in an intercalibration exercise and implementing the above
14 696 recommendations, we find good agreement between the calibrated δ values measured by two
15 697 different IRMS labs for both reference materials and natural lake samples. We conclude that
16 698 while the intercalibration results demonstrate potential for further improvement in precision, the
17 699 intercalibration of $\delta(^{15}\text{N}^{\text{sp}})$ using a uniform scrambling calculation (pyisotopomer) presented here
20 700 represents an improvement upon previous N_2O intercalibrations.

21 701 In this paper, we demonstrate the need to support efforts to generate and distribute
22 702 reference gases to the community. At present, the only commercially available reference
23 703 materials are USGS 51 and USGS 52⁵⁵, which do not have sufficiently distinct values of $\delta(^{15}\text{N}^{\text{sp}})$
24
25 704 to obtain precise values of γ and κ with the algebraic solution unless the user is able to achieve
26 705 extremely small measurement uncertainties in ^{31}R . There have been other efforts to produce
27 706 more calibrated N_2O reference gases⁷⁹, but these gases are not yet commercially available. A
28 707 fully funded program is needed to produce reference materials such as 53504, which —
29 708 combined with reference materials such as USGS 51 and USGS 52 — should provide users with
30 709 precise and accurate N_2O isotopocule calibrations.

32 710

33 711 **Data availability statement**

34 712 The manuscript is prepared to comply with the RCMS data policy. The latest version of
35 713 pyisotopomer is available for installation via the Python Package index
36 714 (pypi.org/project/pyisotopomer). The second release of pyisotopomer is also available via
37 715 Zenodo (doi.org/10.5281/zenodo.7552724). This research was supported by U.S.-NSF grant
38 716 OCE-1657868 to K. L. Casciotti. C. L. Kelly is supported by an NSF Graduate Research
39 717 Fellowship. The authors declare no competing financial interests.

40 717

41

42

43

44

45

46

47

48

49

50

51

52

53

54

55

56

57

58

59

60

718 **References**

- 719
- 720 1. Yung YL, Wang WC, Lacis AA. Greenhouse effect due to atmospheric nitrous oxide.
721 *Geophys Res Lett.* 1976;3(10):619-621. doi:10.1029/GL003i010p00619
- 722 2. Smith C, Nicholls ZRJ, Armour K, et al. The Earth's Energy Budget, Climate Feedbacks,
723 and Climate Sensitivity Supplementary Material. In: Masson-Delmotte V, Zhai P, Pirani A,
724 et al., eds. *Climate Change 2021: The Physical Science Basis. Contribution of Working*
725 *Group I to the Sixth Assessment Report of the Intergovernmental Panel on Climate Change.*
726 Cambridge University Press; 2021. Accessed October 4, 2021.
727 [https://www.ipcc.ch/report/ar6/wg1/downloads/report/IPCC_AR6_WGI_Chapter_07_Sup](https://www.ipcc.ch/report/ar6/wg1/downloads/report/IPCC_AR6_WGI_Chapter_07_Supplementary_Material.pdf)
728 [plementary_Material.pdf](https://www.ipcc.ch/report/ar6/wg1/downloads/report/IPCC_AR6_WGI_Chapter_07_Supplementary_Material.pdf)
- 729 3. Crutzen PJ. The influence of nitrogen oxides on the atmospheric ozone content. *Q J R*
730 *Meteorol Soc.* 1970;96(408):320-325. doi:10.1002/qj.49709640815
- 731 4. Ravishankara AR, Daniel JS, Portmann RW. Nitrous Oxide (N₂O): The Dominant Ozone-
732 Depleting Substance Emitted in the 21st Century. *Science.* 2009;326(5949):123-125.
733 doi:10.1126/science.1176985
- 734 5. Wuebbles DJ. Nitrous Oxide: No Laughing Matter. *Science.* 2009;326(5949):56-57.
735 doi:10.1126/science.1179571
- 736 6. Müller R. The impact of the rise in atmospheric nitrous oxide on stratospheric ozone.
737 *Ambio.* 2021;50(1):35-39. doi:10.1007/s13280-020-01428-3
- 738 7. Kim KR, Craig H. Nitrogen-15 and Oxygen-18 Characteristics of Nitrous Oxide: A Global
739 Perspective. *Science.* 1993;262(5141):1855-1857. doi:10.1126/science.262.5141.1855
- 740 8. Pérez T, Trumbore SE, Tyler SC, Davidson EA, Keller M, Camargo PB de. Isotopic
741 variability of N₂O emissions from tropical forest soils. *Glob Biogeochem Cycles.*
742 2000;14(2):525-535. doi:10.1029/1999GB001181
- 743 9. Kim KR, Craig H. Two-isotope characterization of N₂O in the Pacific Ocean and
744 constraints on its origin in deep water. *Nature.* 1990;347(6288):58-61.
745 doi:10.1038/347058a0
- 746 10. Dore JE, Popp BN, Karl DM, Sansone FJ. A large source of atmospheric nitrous oxide from
747 subtropical North Pacific surface waters. *Nature.* 1998;396(6706):63-66.
748 doi:10.1038/23921
- 749 11. Naqvi SWA, Naik H, Jayakumar A, et al. Seasonal Anoxia Over the Western Indian
750 Continental Shelf. In: Wiggert JD, Hood RR, Naqvi SWA, Brink KH, Smith SL, eds.
751 *Geophysical Monograph Series.* Vol 185. American Geophysical Union; 2009:333-345.
752 doi:10.1029/2008GM000745
- 753 12. Yoshida N, Hattori A, Saino T, Matsuo S, Wada E. 15N/14N ratio of dissolved N₂O in the
754 eastern tropical Pacific Ocean. *Nature.* Published online 1984. doi:10.1038/307442A0

- 1
2
3 755 13. Rahn T, Wahlen M. Stable Isotope Enrichment in Stratospheric Nitrous Oxide. *Science*.
4 756 1997;278(5344):1776-1778. doi:10.1126/science.278.5344.1776
5
6 757 14. Rahn T, Wahlen M. A reassessment of the global isotopic budget of atmospheric nitrous
7 758 oxide. *Glob Biogeochem Cycles*. 2000;14(2):537-543. doi:10.1029/1999GB900070
9
10 759 15. Yoshida N. ¹⁵N-depleted N₂O as a product of nitrification. *Nature*. 1988;335(6190):528-
11 760 529. doi:10.1038/335528a0
12
13 761 16. Barford CC, Montoya JP, Altabet MA, Mitchell R. Steady-State Nitrogen Isotope Effects of
14 762 N₂ and N₂O Production in *Paracoccus denitrificans*. *Appl Environ Microbiol*.
15 763 1999;65(3):989-994. doi:10.1128/AEM.65.3.989-994.1999
16
17 764 17. Pérez T, Trumbore SE, Tyler SC, et al. Identifying the agricultural imprint on the global
18 765 N₂O budget using stable isotopes. *J Geophys Res Atmospheres*. 2001;106(D9):9869-9878.
19 766 doi:10.1029/2000JD900809
20
21
22 767 18. Yamulki S, Toyoda S, Yoshida N, Veldkamp E, Grant B, Bol R. Diurnal fluxes and the
23 768 isotopomer ratios of N₂O in a temperate grassland following urine amendment. *Rapid*
24 769 *Commun Mass Spectrom*. 2001;15(15):1263-1269. doi:10.1002/rcm.352
25
26 770 19. Lewicka-Szczebak D, Augustin J, Gieseemann A, Well R. Quantifying N₂O reduction to N₂
27 771 based on N₂O isotopocules – validation with independent methods (helium incubation and
28 772 ¹⁵N gas flux method). *Biogeosciences*. 2017;14(3):711-732. doi:https://doi.org/10.5194/bg-
29 773 14-711-2017
30
31
32 774 20. Verhoeven E, Barthel M, Yu L, et al. Early season N₂O emissions under variable water
33 775 management in rice systems: source-partitioning emissions using isotope ratios along a
34 776 depth profile. *Biogeosciences*. 2019;16(2):383-408. doi:https://doi.org/10.5194/bg-16-383-
35 777 2019
36
37
38 778 21. Yoshida N, Toyoda S. Constraining the atmospheric N₂O budget from intramolecular site
39 779 preference in N₂O isotopomers. *Nature*. 2000;405(6784):330-334. doi:10.1038/35012558
40
41 780 22. Prokopiou M, Martinerie P, Link to external site this link will open in a new window, et al.
42 781 Constraining N₂O emissions since 1940 using firm air isotope measurements in both
43 782 hemispheres. *Atmospheric Chem Phys*. 2017;17(7):4539-4564. doi:10.5194/acp-17-4539-
44 783 2017
45
46 784 23. Yu L, Harris E, Henne S, et al. The isotopic composition of atmospheric nitrous oxide
47 785 observed at the high-altitude research station Jungfraujoch, Switzerland. *Atmospheric Chem*
48 786 *Phys*. 2020;20(11):6495-6519. doi:10.5194/acp-20-6495-2020
49
50
51 787 24. Toyoda S, Yoshida N, Miwa T, et al. Production mechanism and global budget of N₂O
52 788 inferred from its isotopomers in the western North Pacific. *Geophys Res Lett*. 2002;29(3):7-
53 789 1-7-4. doi:10.1029/2001GL014311
54
55
56
57
58

- 1
2
3 790 25. Popp BN, Westley MB, Toyoda S, et al. Nitrogen and oxygen isotopomeric constraints on
4 791 the origins and sea-to-air flux of N₂O in the oligotrophic subtropical North Pacific gyre.
5 792 *Glob Biogeochem Cycles*. 2002;16(4):12-1-12-10. doi:10.1029/2001GB001806
6
7
8 793 26. Yamagishi H, Westley MB, Popp BN, et al. Role of nitrification and denitrification on the
9 794 nitrous oxide cycle in the eastern tropical North Pacific and Gulf of California. *J Geophys*
10 795 *Res Biogeosciences*. 2007;112(G2). doi:10.1029/2006JG000227
11
12 796 27. Yamagishi H, Yoshida N, Toyoda S, Popp BN, Westley MB, Watanabe S. Contributions of
13 797 denitrification and mixing on the distribution of nitrous oxide in the North Pacific. *Geophys*
14 798 *Res Lett*. 2005;32(4). doi:10.1029/2004GL021458
15
16 799 28. Westley MB, Yamagishi H, Popp BN, Yoshida N. Nitrous oxide cycling in the Black Sea
17 800 inferred from stable isotope and isotopomer distributions. *Deep Sea Res Part II Top Stud*
18 801 *Oceanogr*. 2006;53(17-19):1802-1816. doi:10.1016/j.dsr2.2006.03.012
19
20
21 802 29. Farías L, Castro-González M, Cornejo M, et al. Denitrification and nitrous oxide cycling
22 803 within the upper oxycline of the eastern tropical South Pacific oxygen minimum zone.
23 804 *Limnol Oceanogr*. 2009;54(1):132-144. doi:10.4319/lo.2009.54.1.0132
24
25 805 30. Casciotti KL, Forbes M, Vedamati J, Peters BD, Martin TS, Mordy CW. Nitrous oxide
26 806 cycling in the Eastern Tropical South Pacific as inferred from isotopic and isotopomeric
27 807 data. *Deep Sea Res Part II Top Stud Oceanogr*. 2018;156:155-167.
28 808 doi:10.1016/j.dsr2.2018.07.014
29
30
31 809 31. Bourbonnais A, Letscher RT, Bange HW, et al. N₂O production and consumption from
32 810 stable isotopic and concentration data in the Peruvian coastal upwelling system. *Glob*
33 811 *Biogeochem Cycles*. 2017;31(4):678-698. doi:10.1002/2016GB005567
34
35 812 32. Toyoda S, Yoshida O, Yamagishi H, Fujii A, Yoshida N, Watanabe S. Identifying the
36 813 origin of nitrous oxide dissolved in deep ocean by concentration and isotopocule analyses.
37 814 *Sci Rep*. 2019;9(1):1-9. doi:10.1038/s41598-019-44224-0
38
39
40 815 33. Kelly CL, Travis NM, Baya PA, Casciotti KL. Quantifying Nitrous Oxide Cycling Regimes
41 816 in the Eastern Tropical North Pacific Ocean With Isotopomer Analysis. *Glob Biogeochem*
42 817 *Cycles*. 2021;35(2):e2020GB006637. doi:10.1029/2020GB006637
43
44 818 34. Toyoda S, Kakimoto T, Kudo K, et al. Distribution and Production Mechanisms of N₂O in
45 819 the Western Arctic Ocean. *Glob Biogeochem Cycles*. 2021;35(4):e2020GB006881.
46 820 doi:https://doi.org/10.1029/2020GB006881
47
48
49 821 35. Friedman L, Bigeleisen J. Oxygen and Nitrogen Isotope Effects in the Decomposition of
50 822 Ammonium Nitrate. *J Chem Phys*. 1950;18(10):1325-1331. doi:10.1063/1.1747471
51
52 823 36. Toyoda S, Yoshida N. Determination of nitrogen isotopomers of nitrous oxide on a
53 824 modified isotope ratio mass spectrometer. *Anal Chem*. 1999;71(20):4711-4718.
54 825 doi:10.1021/ac9904563
55
56
57
58
59
60

- 1
2
3 826 37. Brenninkmeijer CAM, Röckmann T. Mass spectrometry of the intramolecular nitrogen
4 827 isotope distribution of environmental nitrous oxide using fragment-ion analysis. *Rapid*
5 828 *Commun Mass Spectrom.* 1999;13(20):2028-2033. doi:10.1002/(SICI)1097-
6 829 0231(19991030)13:20<2028::AID-RCM751>3.0.CO;2-J
- 8
9 830 38. Kaiser J, Brenninkmeijer CAM, Röckmann T. Intramolecular ¹⁵N and ¹⁸O fractionation in
10 831 the reaction of N₂O with O(1D) and its implications for the stratospheric N₂O isotope
11 832 signature. *J Geophys Res Atmospheres.* 2002;107(D14):ACH 16-1-ACH 16-14.
12 833 doi:10.1029/2001JD001506
- 14 834 39. Kaiser J. *Stable Isotope Investigations of Atmospheric Nitrous Oxide.* Johannes Gutenberg
15 835 University of Mainz; 2003. <https://doi.org/10.25358/openscience-3976>
- 17 836 40. Röckmann T, Levin I. High-precision determination of the changing isotopic composition
18 837 of atmospheric N₂O from 1990 to 2002. *J Geophys Res Atmospheres.* 2005;110(D21).
19 838 doi:10.1029/2005JD006066
- 21 839 41. Yung YL, Miller CE. Isotopic Fractionation of Stratospheric Nitrous Oxide. *Science.*
22 840 1997;278(5344):1778-1780. doi:10.1126/science.278.5344.1778
- 25 841 42. Röckmann T, Kaiser J, Brenninkmeijer CAM, et al. Isotopic enrichment of nitrous oxide
26 842 (¹⁵N¹⁴NO, ¹⁴N¹⁵NO, ¹⁴N¹⁴N¹⁸O) in the stratosphere and in the laboratory. *J Geophys*
27 843 *Res Atmospheres.* 2001;106(D10):10403-10410. doi:10.1029/2000JD900822
- 29 844 43. Toyoda S, Yoshida N, Urabe T, et al. Temporal and latitudinal distributions of stratospheric
30 845 N₂O isotopomers. *J Geophys Res Atmospheres.* 2004;109(D8). doi:10.1029/2003JD004316
- 33 846 44. Kaiser J, Engel A, Borchers R, Rockmann T. Probing stratospheric transport and chemistry
34 847 with new balloon and aircraft observations of the meridional and vertical N₂O isotope
35 848 distribution. *Atmos Chem Phys.* Published online 2006:22.
- 37 849 45. Park S, Atlas EL, Boering KA. Measurements of N₂O isotopologues in the stratosphere:
38 850 Influence of transport on the apparent enrichment factors and the isotopologue fluxes to the
39 851 troposphere. *J Geophys Res Atmospheres.* 2004;109(D1). doi:10.1029/2003JD003731
- 41 852 46. Sutka RL, Ostrom NE, Ostrom PH, Gandhi H, Breznak JA. Nitrogen isotopomer site
42 853 preference of N₂O produced by *Nitrosomonas europaea* and *Methylococcus capsulatus*
43 854 Bath. *Rapid Commun Mass Spectrom RCM.* 2003;17(7):738-745. doi:10.1002/rcm.968
- 46 855 47. Sutka RL, Ostrom NE, Ostrom PH, et al. Distinguishing Nitrous Oxide Production from
47 856 Nitrification and Denitrification on the Basis of Isotopomer Abundances. *Appl Environ*
48 857 *Microbiol.* 2006;72(1):638-644. doi:10.1128/AEM.72.1.638-644.2006
- 50 858 48. Sutka RL, Ostrom NE, Ostrom PH, Gandhi H, Breznak JA. Nitrogen isotopomer site
51 859 preference of N₂O produced by *Nitrosomonas europaea* and *Methylococcus capsulatus*
52 860 Bath. *Rapid Commun Mass Spectrom.* 2004;18(12):1411-1412. doi:10.1002/rcm.1482

- 1
2
3 861 49. Toyoda S, Mutobe H, Yamagishi H, Yoshida N, Tanji Y. Fractionation of N₂O isotopomers
4 862 during production by denitrifier. *Soil Biol Biochem.* 2005;37(8):1535-1545.
5 863 doi:10.1016/j.soilbio.2005.01.009
6
7
8 864 50. Frame CH, Casciotti KL. Biogeochemical controls and isotopic signatures of nitrous oxide
9 865 production by a marine ammonia-oxidizing bacterium. *Biogeosciences.* 2010;7(9):2695-
10 866 2709. doi:10.5194/bg-7-2695-2010
11
12 867 51. Lazo-Murphy BM, Larson S, Staines S, et al. Nitrous oxide production and isotopomer
13 868 composition by fungi isolated from salt marsh sediments. *Front Mar Sci.* 2022;9. Accessed
14 869 January 3, 2023. <https://www.frontiersin.org/articles/10.3389/fmars.2022.1098508>
15
16
17 870 52. Ostrom NE, Pitt A, Sutka R, et al. Isotopologue effects during N₂O reduction in soils and in
18 871 pure cultures of denitrifiers. *J Geophys Res Biogeosciences.* 2007;112(G2).
19 872 doi:10.1029/2006JG000287
20
21 873 53. Kaiser J, Park S, Boering KA, Brenninkmeijer CAM, Hilker A, Röckmann T. Mass
22 874 spectrometric method for the absolute calibration of the intramolecular nitrogen isotope
23 875 distribution in nitrous oxide. *Anal Bioanal Chem.* 2004;378(2):256-269.
24 876 doi:10.1007/s00216-003-2233-2
25
26
27 877 54. Westley MB, Popp BN, Rust TM. The calibration of the intramolecular nitrogen isotope
28 878 distribution in nitrous oxide measured by isotope ratio mass spectrometry. *Rapid Commun*
29 879 *Mass Spectrom.* 2007;21(3):391-405. doi:10.1002/rcm.2828
30
31 880 55. Ostrom NE, Gandhi H, Coplen TB, et al. Preliminary assessment of stable nitrogen and
32 881 oxygen isotopic composition of USGS51 and USGS52 nitrous oxide reference gases and
33 882 perspectives on calibration needs. *Rapid Commun Mass Spectrom.* 2018;32(15):1207-1214.
34 883 doi:10.1002/rcm.8157
35
36
37 884 56. Mohn J, Wolf B, Toyoda S, et al. Interlaboratory assessment of nitrous oxide isotopomer
38 885 analysis by isotope ratio mass spectrometry and laser spectroscopy: current status and
39 886 perspectives. *Rapid Commun Mass Spectrom.* 2014;28(18):1995-2007.
40 887 doi:10.1002/rcm.6982
41
42
43 888 57. Kelly CL. pyisotopomer: Nitrous oxide isotopocule data corrections in Python. Published
44 889 online January 5, 2023. Accessed March 13, 2023. <https://pypi.org/project/pyisotopomer/>
45
46
47 890 58. Baertschi P. Absolute ¹⁸O content of standard mean ocean water. *Earth Planet Sci Lett.*
48 891 1976;31(3):341-344. doi:10.1016/0012-821X(76)90115-1
49
49 892 59. Jabeen I, Kusakabe M. Determination of δ ¹⁷O values of reference water samples VSMOW
50 893 and SLAP. *Chem Geol.* 1997;143:115-119. doi:10.1016/S0009-2541(97)00109-5
51
52
53 894 60. Kaiser J, Röckmann T, Brenninkmeijer CAM. Complete and accurate mass spectrometric
54 895 isotope analysis of tropospheric nitrous oxide. *J Geophys Res Atmospheres.*
55 896 2003;108(D15). doi:10.1029/2003JD003613
56
57
58
59
60

- 1
2
3 897 61. Kaiser J, Röckmann T. Correction of mass spectrometric isotope ratio measurements for
4 898 isobaric isotopologues of O₂, CO, CO₂, N₂O and SO₂. *Rapid Commun Mass Spectrom.*
5 899 2008;22(24):3997-4008. doi:10.1002/rcm.3821
6
7 900 62. Kaiser J, Hastings MG, Houlton BZ, Röckmann T, Sigman DM. Triple Oxygen Isotope
8 901 Analysis of Nitrate Using the Denitrifier Method and Thermal Decomposition of N₂O.
9 902 *Anal Chem.* 2007;79(2):599-607. doi:10.1021/ac061022s
10
11 903 63. Wankel SD, Ziebis W, Buchwald C, et al. Evidence for fungal and chemodenitrification
12 904 based N₂O flux from nitrogen impacted coastal sediments. *Nat Commun.* 2017;8(1):1-11.
13 905 doi:10.1038/ncomms15595
14
15 906 64. Magyar PM, Orphan VJ, Eiler JM. Measurement of rare isotopologues of nitrous oxide by
16 907 high-resolution multi-collector mass spectrometry. *Rapid Commun Mass Spectrom.*
17 908 2016;30(17):1923-1940. doi:10.1002/rcm.7671
18
19 909 65. Kelly CL. ckelly314/pyisotopomer: v1.0.4. Published online January 19, 2023.
20 910 doi:10.5281/zenodo.7552724
21
22 911 66. McIlvin MR, Casciotti KL. Technical updates to the bacterial method for nitrate isotopic
23 912 analyses. *Anal Chem.* 2011;83(5):1850-1856. doi:10.1021/ac1028984
24
25 913 67. McIlvin MR, Casciotti KL. Fully automated system for stable isotopic analyses of dissolved
26 914 nitrous oxide at natural abundance levels. *Limnol Oceanogr Methods.* 2010;8(2):54-66.
27 915 doi:10.4319/lom.2010.8.54
28
29 916 68. Scott KM, Lu X, Cavanaugh CM, Liu JS. Optimal methods for estimating kinetic isotope
30 917 effects from different forms of the Rayleigh distillation equation 1 Associate editor: J.
31 918 Horita. *Geochim Cosmochim Acta.* 2004;68(3):433-442. doi:10.1016/S0016-
32 919 7037(03)00459-9
33
34 920 69. LI W. Measurement of the absolute abundance of oxygen-17 in V-SMOW. *Chin Sci Bull.*
35 921 1988;33:1610-1613. Accessed June 10, 2021. <https://ci.nii.ac.jp/naid/80004607415/>
36 922
37 923 70. Santoro AE, Buchwald C, McIlvin MR, Casciotti KL. Isotopic Signature of N₂O Produced
38 924 by Marine Ammonia-Oxidizing Archaea. *Science.* 2011;333(6047):1282-1285.
39 925 doi:10.1126/science.1208239
40 926
41 927 71. Dutton GS, Elkins JW, Hall BD. Nitrous Oxide data from the NOAA/ESRL halocarbons in
42 928 situ program. Published online 2021. Accessed November 19, 2021.
43 929 <https://data.nodc.noaa.gov/cgi-bin/iso?id=gov.noaa.ncdc:C01556>
44 930
45 931 72. Inoue HY, Mook WG. Equilibrium and kinetic nitrogen and oxygen isotope fractionations
46 932 between dissolved and gaseous N₂O. *Chem Geol.* 1994;113(1):135-148. doi:10.1016/0009-
47 2541(94)90009-4
48
49 931 73. Röckmann T, Kaiser J, Brenninkmeijer CAM, Brand WA. Gas chromatography/isotope-
50 932 ratio mass spectrometry method for high-precision position-dependent ¹⁵N and ¹⁸O

- 1
2
3 933 measurements of atmospheric nitrous oxide. *Rapid Commun Mass Spectrom.*
4 934 2003;17(16):1897-1908. doi:10.1002/rcm.1132
5
6 935 74. Glover DM, Jenkins WJ, Doney SC. *Modeling Methods for Marine Science*. Cambridge
7 936 University Press; 2011. doi:10.1017/CBO9780511975721
8
9 937 75. Lorquet JC, Cadet C. Excited states of gaseous ions: I. Selection rules in photoelectron
10 938 spectroscopy and photoionization. The case of N₂O⁺. *Int J Mass Spectrom Ion Phys.*
11 939 1971;7(3):245-254. doi:10.1016/0020-7381(71)80020-7
12
13
14 940 76. Märk E, Märk TD, Kim YB, Stephan K. Absolute electron impact ionization cross section
15 941 from threshold up to 180 eV for N₂O+e⁻→N₂O⁺⁺+2e⁻ and the metastable and collision
16 942 induced dissociation of N₂O⁺. *J Chem Phys.* 1981;75(9):4446-4453. doi:10.1063/1.442611
17
18 943 77. Bigeleisen J. Chemistry of Isotopes. *Science.* 1965;147(3657):463-471.
19 944 doi:10.1126/science.147.3657.463
20
21 945 78. Begun GM, Landau L. Metastable Transitions in N₂O⁺. *J Chem Phys.* 1962;36(4):1083-
22 946 1084. doi:10.1063/1.1732641
23
24 947 79. Mohn J, Biasi C, Bodé S, et al. Isotopically characterised N₂O reference materials for use
25 948 as community standards. *Rapid Commun Mass Spectrom.* 2022;36(13):e9296.
26 949 doi:10.1002/rcm.9296
27
28
29
30 950
31 951

Table 1. Reference materials for N₂O isotopic analysis and intercalibration. Except for one internal standard (B6), calibrated values were provided via independent measurement by S. Toyoda, Tokyo Tech., J. Mohn, EMPA; or, in the case of tropospheric N₂O, the 2018 annual average measured at Jungfraujoch, Switzerland, reported by Yu et al. (2020). The laboratories participating in the intercalibration exercise were at Stanford University (“Lab 1”) and the University of Basel (“Lab 2”). ³¹R values represent the inherent, unscrambled ³¹R of each reference material, calculated from eqn. (6).

Reference material	Matrix	Mole fraction μmol mol ⁻¹	$\delta(^{15}\text{N}^\alpha)$	$\delta(^{15}\text{N}^\beta)$	$\delta(^{15}\text{N}^{\text{sp}})$	$\delta(^{15}\text{N}^{\text{bulk}})$	$\delta(^{18}\text{O})$	^{31}R ($^{15}\text{R}^\alpha + ^{17}\text{R}$)	^{45}R	^{46}R	Calibration by
			(%o, vs. air N ₂)				(%o, vs. VSMOW)				
S2 reference gas	Synthetic air	90	5.55	-12.87	18.42	-3.66	32.73	0.004083	0.007712	0.002087	Toyoda & Mohn
B6 reference gas	He	900	-0.40	-0.15	-0.26	-0.28	41.95	0.004063	0.007739	0.002106	Lab 1 internal standard
Tropospheric N ₂ O (2018 annual average)	Air	~0.33	15.6	-2.3	17.9	6.6	44.4	0.004123	0.007787	0.002111	Yu et al. (2020)
CA06261	Synthetic air	90	-22.21	-49.28	27.07	-35.75	26.94	0.003980	0.007475	0.002075	Toyoda & Mohn
53504	Synthetic air	90	1.71	94.44	-92.73	48.08	36.01	0.004070	0.008093	0.002095	Toyoda & Mohn
CA08214	Synthetic air	90	17.11	-3.43	20.54	6.84	35.39	0.004126	0.007790	0.002093	Toyoda & Mohn
90454	Synthetic air	90	25.73	25.44	0.29	25.59	35.88	0.004158	0.007928	0.002094	Toyoda & Mohn
94321	Synthetic air	90	50.52	2.21	48.31	26.37	35.54	0.004249	0.007934	0.002094	Toyoda & Mohn
Lab 1 pure N ₂ O direct injection ("A01")	Pure N ₂ O	N/A	0.24	0.12	0.13	0.18	39.85	0.003734	0.007742	0.002101	Toyoda
Lab 2 pure N ₂ O direct injection	Pure N ₂ O	N/A	-4.07	3.59	-7.66	-0.24	39.25	0.004044	0.007739	0.002100	Mohn

958
959

Table 2. N₂O isotopic composition of reference materials and two unknowns analyzed by two IRMS laboratories, calculated using γ and κ values determined from reference materials 53504 and CA08214 with the algebraic solution. $\delta(^{15}\text{N}^\alpha)$, $\delta(^{15}\text{N}^\beta)$, $\delta(^{15}\text{N}^{\text{sp}})$ and $\delta(^{15}\text{N}^{\text{bulk}})$ are reported in ‰ vs. Air N₂, and $\delta^{18}\text{O}$ is reported in ‰ vs. VSMOW. Uncertainties are standard deviations of replicate bottles and do not include calibration uncertainties. The root-mean square deviation (RMSD) was calculated with respect to calibrated values.

Reference material		<i>n</i>	$\delta(^{15}\text{N}^\alpha)$	σ	$\delta(^{15}\text{N}^\beta)$	σ	$\delta(^{15}\text{N}^{\text{sp}})$	σ	$\delta(^{15}\text{N}^{\text{bulk}})$	σ	$\delta(^{18}\text{O})$	σ
			(‰, vs. air N ₂)						(‰, vs. VSMOW)			
CA06261	Calibrated value		-22.2		-49.3		27.1		-35.7		26.9	
	Lab 1	4	-20.6	1.3	-50.5	1.3	29.9	2.7	-35.6	0.2	28.4	0.8
	Lab 2	16	-20.5	1.4	-50.9	2.6	30.4	3.8	-35.7	1.0	27.6	1.8
	RMSD		2.3		2.1		4.4		0.2		1.5	
53504	Calibrated value		1.7		94.4		-92.7		48.1		36.0	
	Lab 1	4	0.0	1.0	95.7	2.1	-95.7	2.5	47.9	1.1	37.6	0.8
	Lab 2	15	1.7	1.0	94.5	1.9	-92.8	2.9	48.1	0.6	36.4	1.6
	RMSD		1.7		1.3		3.0		0.2		1.7	
CA08214	Calibrated value		17.1		-3.4		20.5		6.8		35.3	
	Lab 1	6	17.0	2.0	-2.4	0.9	19.4	2.9	7.3	0.7	36.3	1.4
	Lab 2	16	17.0	1.1	-3.2	0.7	20.2	1.3	6.9	0.6	36.0	3.6
	RMSD		0.1		1.1		1.2		0.5		1.3	
Tropospheric N ₂ O	Calibrated value		15.6		-2.3		17.9		6.6		44.4	
	Lab 1	7	15.1	0.8	-2.5	2.3	17.5	2.8	6.3	1.0	43.1	2.1
	Lab 2	2	15.8	1.1	-3.7	0.0	19.5	1.0	6.1	0.5	44.7	1.0
	RMSD		0.6		1.4		1.7		0.6		1.3	
B6	Calibrated value		-0.4		-0.1		-0.3		-0.3		41.9	
	Lab 1	7	-2.2	0.7	1.3	1.0	-3.4	1.2	-0.4	0.7	41.5	1.6
	RMSD		1.8		1.4		3.2		0.2		0.5	
S2	Calibrated value		5.6		-12.9		18.4		-3.7		32.7	
	Lab1	6	5.0	0.5	-13.1	1.6	18.1	1.3	-4.0	1.0	31.5	1.8
	RMSD		0.5		0.2		0.3		0.4		1.2	
Lake Lugano, 10m	Lab 1	3	13.2	0.3	-5.6	1.2	18.8	1.5	3.8	0.4	44.6	1.2
	Lab 2	5	14.8	1.5	-6.6	1.3	21.4	2.5	4.1	0.5	45.5	0.6
Lake Lugano, 90m	Lab 1	3	19.2	0.5	-33.1	0.7	52.3	1.2	-6.9	0.1	56.8	0.1
	Lab 2	2	18.5	0.8	-32.4	0.3	50.9	0.5	-6.9	0.5	55.4	1.9

966